Available online at www.sciencedirect.com
ScienceDirect
Lithos 92 (2006) 484–505
LITHOS
www.elsevier.com/locate/lithos

Ultra high temperature-metamorphism and its significance in the Central Indian Tectonic Zone

Santanu Kumar Bhowmik

Department of Geology & Geophysics, Indian Institute of Technology, Kharagpur-721 302, India

Received 20 May 2005; accepted 30 March 2006
Available online 23 August 2006

Abstract

In the present study from the southern margin of the Central Indian Tectonic Zone, it is demonstrated how the metamorphic *P*–*T* path of ultrahigh-temperature granulite terranes can be reconstructed using the metamorphic transition in corundum granulites from early biotite melting to later FMAS solid–solid reaction. The extreme metamorphism in these rocks caused two-stage biotite melting, resulting in initial porphyroblastic garnet$_1$ and later sapphirine–spinel$_1$ incongruent solid mineral assemblages. During this process, the leucocratic and melanocratic layers in the corundum granulites evolved from an initial silica-oversaturated to a later silica-undersaturated domain. In the melanocratic layer, this allowed localized concentration of sapphirine-spinel$_1$ and residual sillimanite$_1$, producing an extremely restitic assemblage, at the culmination of peak metamorphism, BM$_1$. BM$_1$ is constrained at ~1000 °C at relatively deep crustal levels (P~9 kbar) from the stability of ferroaugite in a co-metamorphosed Iron Formation granulite. During subsequent metamorphism (BM$_2$), the reaction path and history in the corundum granulites shifted to the restitic domain allowing reacting sapphirine, spinel$_1$ and sillimanite to produce coronal garnet$_2$–corundum assemblage via a FMAS univariant reaction. In the final stages of reaction history, biotite$_2$–sillimanite$_2$–spinel$_2$ assemblage was produced after garnet$_2$–corundum due to localized melt–crystal interaction. The metamorphic sequence, when interpreted with the help of a newly constructed, qualitative KFMASH petrogenetic grid, reveals successive stages of heating, increasing pressure and cooling around the KFMASH invariant point, [Opx,Crd], which is consistent with a counterclockwise metamorphic *P*–*T* path. The near isobaric nature of post-peak cooling (ΔT~250–300 °C) is also evident from multistage pyroxene exsolution and by the appearance of lamellar and coronal garnets in the Iron Formation granulites. This study provides the first tight constraint for ultrahigh-*T* metamorphism along a counter clockwise *P*–*T* trajectory in the Central Indian Tectonic zone, and has important bearing for terrane correlations in this part of East Gondwanaland. In addition, the new KFMASH grid allows evaluation of metamorphic phase relations in ultrahigh-*T*, corundum-bearing and corundum-absent aluminous granulites.

Keywords: Central Indian Tectonic Zone; UHT metamorphism; Corundum granulite; KFMASH grid

1. Introduction

Recent progress in understanding experimental constraints of biotite melting reactions (Carrington and Harley, 1995; Nair and Chacko, 2002) as well as refinements in geothermobarometers (Pattison et al., 2003) for common pelitic and felsic gneiss bulk rock compositions has allowed ultra high temperature metamorphism (UHT, T~900–1150 °C at P~7–10 kbar; Harley, 1998a, 2004) to be increasingly recognized in

E-mail address: Santanu.Kumar.Bhowmik@iitkgp.ac.in.

0024-4937/$ - see front matter © 2006 Elsevier B.V. All rights reserved.
doi:10.1016/j.lithos.2006.03.061

different metamorphic belts, worldwide. This allows for insight into the metamorphic response to the extreme thermal conditions that existed in the continental crust at different points of Earth's history. The bulk of these studies have been made in silica-oversaturated high-Mg–Al granulites, particularly from KFMASH [Bt] absent mineral assemblages, which reveal post-peak isobaric cooling (IBC) (Ellis et al., 1980; Harley, 1985; Sandiford et al., 1987; Currie and Gittins, 1988), isothermal decompression (ITD) (Droop, 1989; Harley et al., 1990; Bertrand et al., 1992; Ouzegane and Bouzame, 1996; Raith et al., 1997; Harley, 1998b; Sajeev et al., 2004) and composite IBC–ITD (Sengupta et al., 1990; Dasgupta et al., 1995; Sajeev and Osanai, 2004; Goncalves et al., 2004) metamorphic *P–T* paths. Although the first two are generally modelled in terms of overall anticlockwise and clockwise metamorphic *P–T* paths respectively, in the majority of these studies, the prograde segment has been rarely documented (e.g. Motoyoshi and Matsueda, 1984; Motoyoshi and Hensen, 1989; Sengupta et al., 1990; Dasgupta et al., 1995). This becomes significant in the light of the polymetamorphic history for large numbers of UHT terrains and where the second granulite facies event is also at high temperatures (e.g. Dasgupta et al., 1995; Goncalves et al., 2004). All these complicate the metamorphic reconstruction of the early UHT event.

Several recent studies also indicate that the silica-undersaturated corundum-bearing granulites are quite robust in constraining the *P–T–X* history of the UHT granulites (Ouzegane et al., 2003; Kelly and Harley, 2004). Given the general modification of aluminous

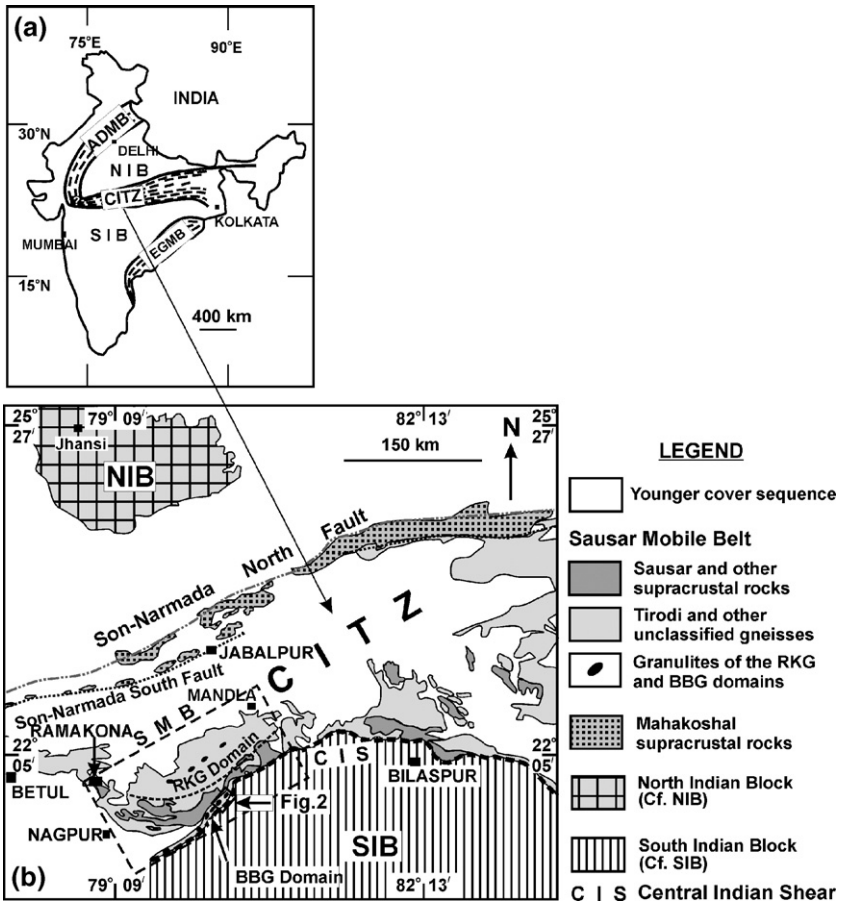

Fig. 1. (a) Location of the Central Indian Tectonic Zone (CITZ) in the tectonic framework of Peninsular India. EGMB (Eastern Ghats Mobile Belt) and ADMB (Aravalli–Delhi Mobile Belt) represent two contiguous mobile belts. (b) Distribution of the different lithotectonic components in the Central Indian Tectonic Zone (CITZ) between the North Indian Block (NIB) and the South Indian Block (SIB). The dashed rectangle shows the location of the Sausar Mobile Belt (SMB) in the CITZ. SMB comprises two granulite domains, the Ramakona–Katangi granulite (RKG) domain along its northern margin and the Bhandara–Balaghat granulite (BBG) domain along its southern margin. The small box shows the location of the study area in the BBG domain (detailed map shown in Fig. 2a).

protoliths from initial quartz-bearing to quartz-absent mineral assemblages through melting and melt removal (McDade and Harley, 2001; Topuz et al., 2004), the silica-undersaturated granulites are potential rocks that may be potentially integrated into the metamorphic processes responsible for the UHT event.

In the present study, an attempt is made to constrain the prograde, peak and retrograde metamorphic stages of an UHT event, by studying corundum-bearing aluminous granulites (corundum granulites from now on) from the southern margin of the Central Indian Tectonic Zone. A KFMASH petrogenetic grid has been newly constructed within the framework of the present study. This petrogenetic grid was used to tightly constrain the metamorphic P–T path for this UHT event. In addition, the extreme thermal conditions for the metamorphism and the post-peak IBC P–T path have been constrained using a co-metamorphosed Iron Formation granulite. Because of its critical position in the tectonic framework of East Gondwanaland, these new findings in the Central Indian Tectonic Zone have important implications for modeling lower crustal geodynamic processes, in general, and in Precambrian crustal reassembly, in particular.

2. Geological background

Samples for metamorphic studies in this work come from the Bhandara–Balaghat granulite (BBG) domain, at the southern periphery of the Sausar Mobile Belt (SMB) (Fig. 1). The latter constitutes the southern component of the composite Central Indian Tectonic Zone (CITZ) (Fig. 1). In recent reconstructions of East Gondwanaland, the CITZ has been recognized as an important Proterozoic collisional zone, along which the North Indian Block (NIB, Eriksson et al., 1999 and comprising the Aravalli–Bundelkhand Provinces) and the South Indian Block (SIB), comprising the Singhbhum, Bastar and Dharwar Provinces are suggested to have been amalgamated during the Palaeoproterozoic to form the Indian subcontinent (Yedekar et al., 1990; Jain et al., 1991; Mishra et al., 2000). Recent metamorphic studies in the SMB reveal contrasting tectonothermal histories and a polycyclic evolutionary history for the orogen (Table 1). A regional high-pressure metamorphic event along a clockwise P–T path, of possible Mesoproterozoic age, has been established from its northern Ramakona–Katangi granulite (RKG) domain. Whereas from the southern Bhandara–Balaghat granulite (BBG) domain, a polymetamorphic evolutionary history, involving a Palaeoproterozoic ultrahigh temperature (UHT) metamorphism and its subsequent reworking in the Meso- and Neoproterozoic, has been recorded.

The 190 km long and 4–20 km wide BBG domain is an allochthonous tectonic sheet between a low-grade (greenschist facies) supracrustal sequence (Sausar Group of rocks) in the north and the SIB on the south (Fig. 2) (Bhowmik and Pal, 2000; Bhowmik and Roy, 2003; Bhowmik et al., 2005). Its northern and southern margins are marked by ductile shear zones. A granulite facies supracrustal suite of garnet–cordierite gneiss, Iron Formation granulite, quartzite, corundum granulite and felsic granulite occur as detached lensoid bodies, ~500–1000 m long and ~50–200 m wide within a vast, soil-covered tract. Wherever host rocks are exposed, the granulites are found to occur within granite gneisses, locally migmatitic and garnetiferous. In the majority of the exposures, the supracrustal granulites are interlayered with a mafic–ultramafic magmatic suite of metagabbro, metanoritic gabbro, metanorite, and metaorthopyroxenite. The latter occur as concordant, sheet-like bodies within the granulites. With respect to exposure, the granulites and magmatic rocks occur in ~1:1 volume ratios. There is distinct spatial organization of the supracrustal granulites and the associated magmatic rocks. The gabbroic suite (metagabbro–metanoritic gabbro) is always spatially associated with the felsic granulite–aluminous granulite, Iron Formation granulite rock association in the southern part of the BBG domain. In contrast, the noritic suite (metanorite–metaorthopyroxenite) is always interlayered with garnet–cordierite gneiss and is confined in the northern part of the BBG domain.

Five phases of deformation (BD_1–BD_5, where B refers to the BBG domain) and four phases of metamorphism (BM_1 to BM_4) have been recently suggested for the BBG domain (Bhowmik et al., 2005). The earliest deformation (BD_1) is synchronous with BM_1 granulite facies metamorphism and produced a stromatic migmatite-banding (BS_1) in the felsic, corundum– and garnet–cordierite granulites. Subsequent shear zone deformations (BD_2 to BD_5) significantly attenuated and flattened the BS_1 banding, leading to pervasive recrystallisation and neo-mineralisation. Applying electron microprobe dating (EMP) techniques to monazites, Bhowmik et al. (2005) interpreted the four phases of metamorphism to belong to two temporally separate metamorphic events. The first event at 2040–2090 Ma caused ultrahigh temperature (UHT) metamorphism (T ~ 950 °C) at relatively deeper crustal levels (P ~ 9 kbar) and a subsequent post-peak near isobaric cooling P–T history (BM_2). During the second granulite event at 1525–1450 Ma, the Palaeoproterozoic

Table 1
Contrasting tectonothermal histories in the Sausar Mobile Belt

Location/area	Mineral assemblage, compositional feature, P–T conditions of metamorphism			Metamorphic P–T path	Other features
	Prograde	Peak	Retrograde		
BBG domain					
Palaeoproterozoic event		BM_1	BM_2	Heating–cooling P–T path (CCW?)	Allochthonous polycyclic domain; UHT metamorphism in the Palaeoproterozoic, coincident with layered intrusions of the gabbroic suite; post-peak garnet formation reaction textures common; reworking of the UHT granulites by the Mesoproterozoic granulite event; deformed and metamorphosed mafic dykes present.
Southern part					
[1]Felsic granulite	Bt_1+Pl_1+Qtz	$Grt_1(35, 03)+Opx(58–61, 4–6)$			
[1]Corundum granulite	Bt_1+Sil_1+Qtz, $Bt_1(81)+Grt_1(35–41, 03)+Sil_1$	$Spr(73)+Spl_1(25)+Sil_1$ $P\sim 9$ kbar, 950 °C	Early $Grt_2(38,03)+Crn$ and later $Bt_2+Spl_2(31–33)+Sil_2$ IBC, $T\sim 700$ °C		
Northern part					
[2]Garnet–cordierite gneiss	Bt_1+Sil_1+Qtz	Early Grt(30, 03)–Crd(80) and later Hc(15)–Qtz $P\sim 6$ kbar, 850–900 °C	$Grt_2(18–28,03)+Sil_2$, Bt_2+Sil_2+Qtz IBC, $T\sim 650$ °C		
Mesoproterozoic event		BM_3	BM_4		
Southern part					
[1]Felsic granulite		Opx_2+Pl_2	$Grt_2(23–28,09–11)+Qtz$	Decompression (?) followed by near isothermal loading	
[1]Gabbronorite dyke		$P\sim 6$ kbar, 675 °C	$P\sim 8$ kbar, 675 °C		
RKG domain					
Meso-Neoproterozoic event	RM_0	RM_1	RM_2 and RM_3		
[3]Metapelite granulite	St+Qtz, Early Ky, Bt+Sil_1+Qtz Growth zoning in Grt	Grt (42,07)–Sil_1 $P\sim 9.5$ kbar, $T\sim 850$ °C	An_{90}, Spl(23–26)–Crd(80–83)–An_{90} (RM_2) $P\sim 6$ kbar, $T\sim 825$ °C Ath(63)+Crd(81), Mag+Sil_2, Hög+Mag (RM_3) IBC, $T\sim 600$ °C	CW P–T path having prograde, peak, post-peak ITD and post-decompressional IBC segments	Monocyclic domain (?), regional high-pressure metamorphism during the Mesoproterozoic collisional orogeny; post-peak garnet-breakdown reaction textures common; low-P event coincident with mafic dyke emplacement and felsic plutonism.
[4]Mafic granulite	$Hbl_1(46–51)+Pl_1(An_{54–62})$+Ilm Growth zoning in Grt	Grt(8–10,33–38)+Cpx(51–66,2)+Ru±Qtz $P\sim 9$–10 kbar, $T\sim 750$–800 °C	$Cpx_2(61–63,2–4)–Pl_2(An_{90})–Hbl_2(38)$ (RM_2) $Hbl_2(44–46)–Pl_2$ (RM_3) P~6kbar, T~650°C		
[4]Garnetiferous amphibolite	$Hbl_1(39–53)+Pl_1(An_{57})+Ilm_1$	Grt(10–12, 22–29)+Qtz+Ttn $P\sim 8$ kbar, $T\sim 675$ °C	$Ilm_2+Pl_2(An_{89–94})+Qtz$ ±$Hbl_2(40–56)$ (RM_2) $P\sim 6.4$ kbar, $T\sim 700$ °C		

Data Source- [1]: Bhowmik et al. (2005); [2]: author's unpublished data; [3]: Bhowmik and Spiering, 2004; [4]: Bhowmik and Roy (2003); mineral abbreviations used in this and other tables are after Kretz (1983) unless stated; BBG: Bhandara–Balaghat granulite; RKG: Ramakona–Katangi granulite; (RKG); mineral compositions in Grt and Pyroxenes: from left to right numbers refer Prp and Grs mole % in Grt and Mg No. ($X_{Mg}\times 100$) and wt.% Al_2O_3 content in pyroxenes respectively; for other ferromagnesian phases: numbers refer Mg No. values; subscripts 1, 2 etc. in minerals refer to different generations of its stability; BM/RM: Metamorphic stages in the BBG and the RKG domains respectively; CCW/CW: counter clockwise and clockwise; IBC/ITD: isobaric cooling/isothermal decompression; UHT: ultra-high temperature metamorphism.

granulites experienced crustal attenuation to ~6.4 kbar at $T \sim 675$ °C during BM_3 and subsequent near isothermal loading to ~8 kbar during BM_4.

Samples for the present study were collected from two locations in the Larsara and Pipariya exposures (Fig. 2), particularly from relatively strain shadow domains in the BS_1 foliation. Samples of the Iron Formation granulite were taken from Larsara area, where it occurs as detached bands within the felsic granulite. The chosen sample (sample no. B46A) is coarse-grained and shows a pervasive gneissic banding, defined by alternate quartz-rich, pyroxene-rich and magnetite-rich bands. In the pyroxene-rich band, extremely coarse pyroxene porphyroclasts (5–13 mm long) are aligned parallel to the BS_1//BS_3 foliation. The mineral assemblage of this sample, particularly the high modal quartz and magnetite contents, together with compositional banding, is consistent with a sedimentary precursor for this rock similar to the Fe-rich pyroxene granulites from the Achaean Napier Complex as described by Grew (1982), Sandiford and Powell (1986) and Harley (1987). The samples of the corundum granulites were taken from Pipariya (sample no. B7B) and Larsara exposures (sample no B220D). With regard to the former, the granulites occur as ~20 m long, ~5–10 m wide discontinuous layers, bounded on both sides by metagabbros. In the Larsara outcrop, the corundum granulite occurs as 10 m long and 5 m wide lensoidal bodies within the felsic granulites, in close proximity to the metagabbros. With regard to the latter, two thin sections (B220D(1) and B220D(5)), representing two continuous parts of a BS_1 migmatite banding, are the same as described by Bhowmik et al. (2005). These are used in this study to investigate new microstructural and textural data for the mineralogical evolution of the corundum granulites, and complement a previous study (Bhowmik et al., 2005). For the construction of the KFMASH grid, the relevant mineral chemistry data are taken from Bhowmik et al. (2005).

3. Analytical methods

Mineral chemical data for the Iron Formation granulite was determined using a CAMECA SX-100 electron microprobe at the laboratory of the

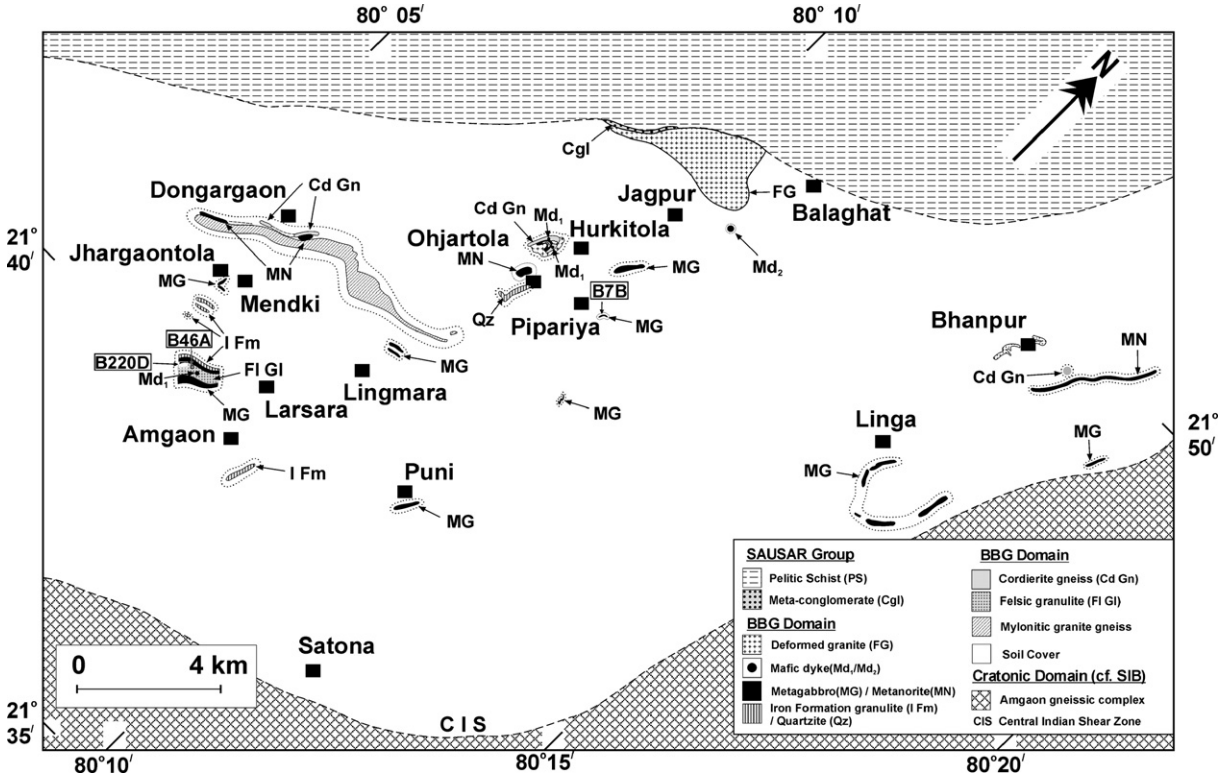

Fig. 2. Simplified lithological map of the Bhandara–Balaghat granulite domain in the SMB. Dotted line indicates the limits of exposure in the soil-covered tract. Also shown are the sample locations of the two study areas: Larsara and Pipariya.

Geological Survey of India at Kolkata, equipped with four WD-spectrometers. The operating conditions were set as 1 μm beam diameter, 15 kV accelerating voltage and 12 nA beam current. Natural and synthetic minerals were used as standards. These were: oxides (Fe, Mn, Ti, Al, Cr), orthoclase (K), albite (Na and Si), andradite (Ca) and olivine (Mg). Representative mineral compositions are given in Table 2. Fe^{3+} was estimated by normalization to the sum of cations per formula and charge balance.

4. Petrology

4.1. Iron Formation granulite

Pyroxenes occur in two textural modes in this sample: (1) type 1 pyroxenes (both ortho- and clinopyroxenes) are 5–13 mm long porphyroclasts, showing multistage exsolution lamellae, pre-dating later deformations. (2) Type 2 pyroxenes occur as smaller strain-free recrystallised grains around type 1 pyroxenes. The

Table 2
Representative electron microprobe analyses of minerals from Iron Formation granulite, corundum granulite and felsic granulite

	Iron Formation granulite						*Corundum granulite					*Felsic granulite
Sample no.	B46A						B220D(5)			B220D(1)		B220A(1)
Mineral	Cpx	Opx	Aug	Grt	Grt	Pl	Grt	Grt	Spl_1	Spr	Bt_1	Opx
Textural	Host	Lam_2	Bulk	Cor	Lam	M	G_1(C)	G_2(C)	I^Per	I^G_2	I^G_1	P(C)
Site												
SiO_2	48.99	47.74	48.77	37.14	36.81	55.90	38.94	38.51	0.05	13.82	37.73	49.63
TiO_2	0.30	0.09	0.26	0.04	–	0.02	–	–	–	0.06	3.76	0.07
Al_2O_3	2.56	1.34	2.35	20.98	20.35	27.27	22.49	22.50	59.19	61.31	16.72	5.63
Cr_2O_3	–	–	–	–	–	–	0.05	–	0.93	0.17	0.13	0.11
FeO	16.61	36.49	20.09	29.78	31.47	0.34	26.36	26.78	29.41	9.58	7.97	23.48
MnO	0.17	0.41	0.21	0.92	1.32	0.01	0.45	0.38	0.02	–	0.02	0.08
MgO	8.83	11.54	9.30	2.50	1.88	–	11.07	9.82	5.46	14.70	18.75	20.36
CaO	20.81	0.70	17.29	8.27	7.30	9.64	1.15	0.86	0.04	0.01	0.02	0.11
Na_2O	0.52	0.05	0.44	–	–	5.97	–	–	–	0.02	0.11	0.02
K_2O	–	0.01	–	–	–	0.10	–	–	–	–	10.16	0.01
ZnO	–	–	–	–	–	–	–	–	4.07	–	0.03	–
BaO	–	–	–	–	–	–	–	–	–	–	0.65	–
Total	98.79	98.37	98.71	99.63	99.13	99.25	100.51	98.85	99.17	99.67	96.05	99.50
(O)	6	6	6	12	12	8	12	12	4	20	22	6
Si	1.907	1.943	1.913	2.966	2.979	2.531	2.949	2.982	0.001	1.662	5.448	1.862
Ti	0.009	0.003	0.008	0.002	–	0.001	–	–	–	0.005	0.408	0.002
Al	0.118	0.064	0.109	1.975	1.941	1.456	2.007	2.054	1.970	8.693	2.846	0.249
Cr^{3+}	–	–		–	–	–	0.003	–	0.021	0.016	0.015	0.003
$^{\#}Fe^{3+}$	0.089	0.049	0.083	0.088	0.101	0.013	0.092	–	–	–	–	0.022
Fe^{2+}	0.452	1.193	0.576	1.901	2.029	–	1.577	1.734	0.695	0.964	0.963	0.715
Mn	0.006	0.014	0.007	0.062	0.090	–	0.029	0.025	–	–	0.002	0.003
Mg	0.513	0.700	0.544	0.298	0.227	–	1.250	1.134	0.230	2.635	4.036	1.138
Ca	0.868	0.031	0.727	0.708	0.633	0.468	0.093	0.071	0.001	0.001	0.003	0.004
Na	0.039	0.004	0.033	–	–	0.524	–	–	–	0.005	0.031	0.001
K	–	–	–	–	–	0.006	–	–	–	–	1.872	–
Zn	–	–	–	–	–	–	–	–	0.085	–	0.003	–
Ba	–	–	–	–	–	–	–	–	–	–	0.037	–
Sum	4.001	4.001	4.000	8.000	8.000	4.999	8.000	8.000	3.003	13.981	15.664	3.999
X_{Mg}	0.532	0.370	0.486						0.249	0.732	0.807	0.614
$X_{Adr+Uvr}$				0.044	0.051		0.031	0.000				
X_{Prp}				0.100	0.076		0.424	0.382				
X_{Alm}				0.641	0.681		0.535	0.585				
X_{Sps}				0.021	0.030		0.010	0.008				
X_{Grs}				0.194	0.162		0.000	0.024				
X_{An}						0.469						

*Data source from Bhowmik et al. (2005); $^{\#}Fe^{3+}=Fe^{3+}$calculated by charge balance; $X_{Mg}=(Mg/(Mg+Fe^{2+})$; G_1–G_2: $garnet_1$–$garnet_2$ (see text); C: core; M: matrix; I: inclusion; Lam=lamellae; Cor: corona; Per: perthite.

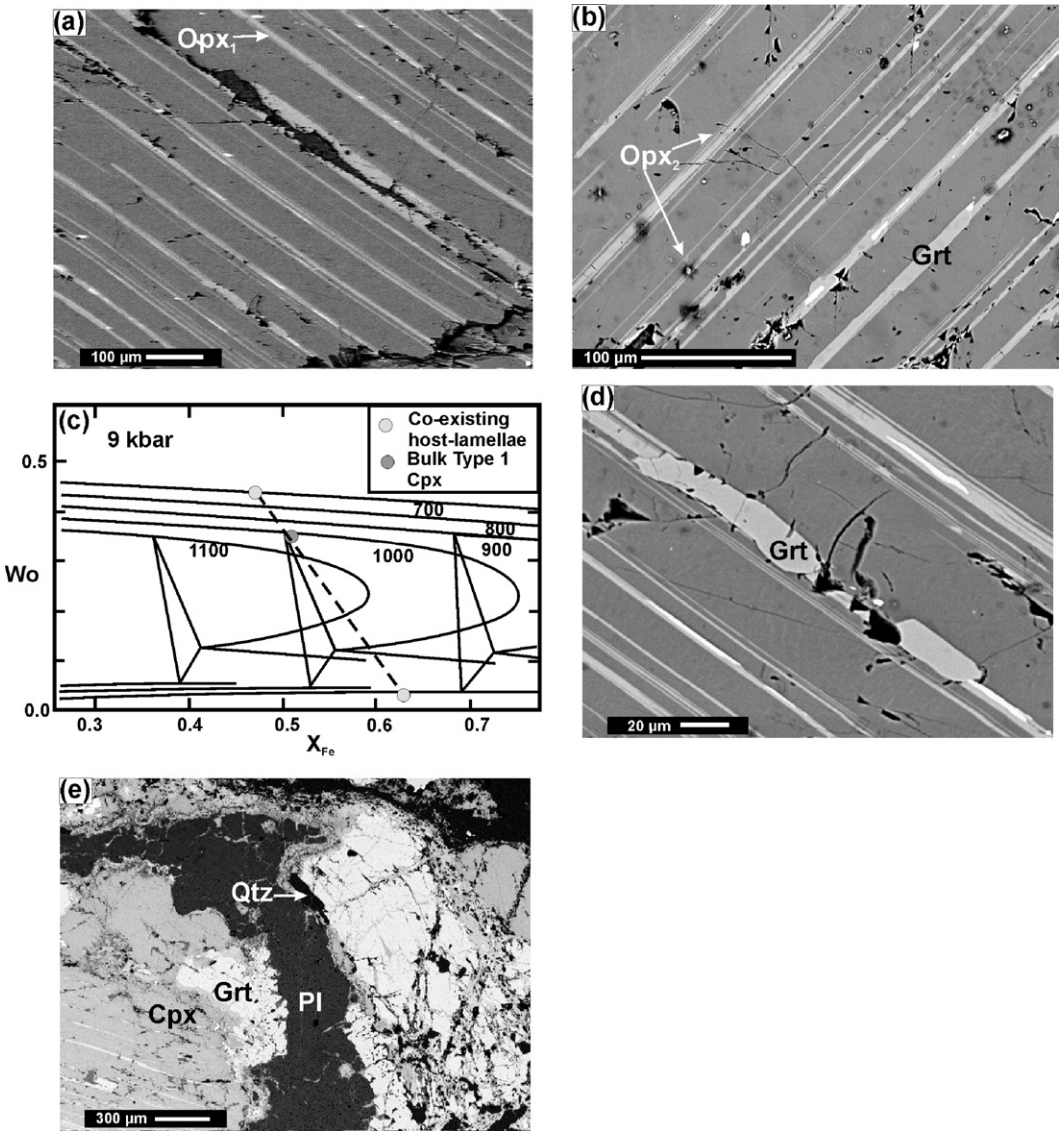

Fig. 3. Backscattered electron images (a–b) and (d–e) and pyroxene quadrilateral diagram (c), showing textures and mineral compositions related to the ultrahigh-*T* metamorphism in the Iron Formation granulite. (a) Type 1 clinopyroxene (darker) showing regular, 10–17 μm thick (100) lamellae of Opx_1 (brighter). (b) A second-stage exsolution in Opx_1, producing 2–3 μm thick Cpx, which alternates with Opx host. Opx_2 lamellae are also exsolved in the Cpx host. Note lamellar garnet in the lower right corner of the photograph. (c) Pyroxene quadrilateral showing the compositions of co-existing Opx lamellae and Cpx host. Also shown is the reconstructed composition of type 1 Cpx (ferroaugite) before exsolution. (d) Lamellar Grt truncating the exsolution lamellae of Opx and Cpx. (e) Coronal Grt–Qtz symplectites at the contact of Cpx and Pl.

UHT metamorphic conditions are constrained from type 1 clinopyroxene. Two stages of exsolution are recognized. The exsolutions of the first stage are 10–17 μm thick (100) lamellae of first generation orthopyroxene (orthopyroxene$_1$) (Fig. 3a). These lamellae are regularly spaced (distance 40–50 μm) within the host clinopyroxene. Orthopyroxene$_1$ consists of second-generation (100) lamellae of ~2–3 μm thick orthopyroxene$_2$ (Wo=1.6; X_{Mg}=0.37; where $X_{Mg}=(Mg/Mg+Fe^{2+})$) and clinopyroxene (Wo=41.6; X_{Mg}=0.53) (Table 2) (Fig. 3b). Thin (2–3 μm thick) orthopyroxene$_2$ also occurs within the clinopyroxene host. Applying modal analysis of lamellae and host, the bulk compositions of the type 1 clinopyroxene is estimated as ferroaugite (Wo=39.4; X_{Mg}=0.485). The reintegrated composition is subject to uncertainties in wollastonite contents

because of possible variations in lamellae geometry, density and late granular exsolution. Because of the presence of non-quadrilateral components (e.g. Al), the thermodynamically corrected compositions of these pyroxenes (after the scheme Andersen et al., 1993 and using the QUILF95 program) are shown in Fig. 3c. The tie line connecting the orthopyroxene$_2$ lamellae and the clinopyroxene host has a shallower slope and is rotated anticlockwise, relative to the experimentally determined high-temperature tie line (Lindsley, 1983). Type 1 orthopyroxenes (1–10 mm long) also show 10–20 μm thick (100) clinopyroxene exsolution lamellae. However, because of later deformation and alterations, the pre-exsolution composition of the type 1 orthopyroxenes could not be estimated. Garnet occurs in two textural modes in the rock, as (i) 10–16 μm thick and 70–85 μm long discontinuous lamellae, wedge-shaped and coincident with the orthopyroxene$_1$ lamellae in the host clinopyroxene (Fig. 3b,d) and as (ii) a layered garnet–quartz corona around the clinopyroxene porphyroclast in contact with the matrix plagioclase (Fig. 3e). In the first mode, the truncation of the orthopyroxene$_2$ and the clinopyroxene lamellae in former orthopyroxene$_1$ suggests further post-exsolution growth of the garnet (Fig. 3d). The composition of the garnet varies from $Prp_{08}Alm_{68}Sps_{03}Grs_{16}Adr_{05}$ (lamellar mode) to $Prp_{10}Alm_{64}Sps_{02}Grs_{19}Adr_{05}$ (coronal mode). Matrix plagioclase is labradorite (X_{An}=0.53).

4.2. Corundum granulite

These rocks are well banded and composed of alternate leucocratic and melanocratic layers. The leucocratic layers are composed of porphyroblastic garnet–perthite–rutile–biotite±quartz±sillimanite±plagioclase±spinel associations. In the melanocratic layers, garnet–spinel–sillimanite–corundum±sapphirine–plagioclase–perthite–biotite associations are present. Petrological relationships in the Pipariya outcrop are shown in Fig. 4. The BS$_1$ banding in this outcrop is composed of alternate garnet–spinel–sillimanite–corundum–biotite–plagioclase–perthite, garnet–perthite–quartz–biotite–sillimanite and quartz–rich bands (Fig. 4). In the garnet–perthite–quartz–biotite–sillimanite layer, approximately 15 vol.% of the perthite–quartz assemblage occurs at the interstices of porphyroblastic garnet. Following Bhowmik et al. (2005), porphyroblastic garnet is referred to as garnet$_1$. In several places, these occur as a 10–50 mm long interconnected network at high angle to the BS$_1$ banding. Quartz occurs as 10–15 vol.% of the perthite–quartz assemblage. Following

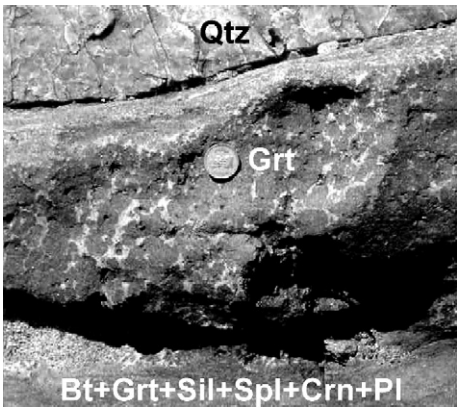

Fig. 4. Field photograph of the Pipariya exposure showing the development of leucosomes in the compositionally banded corundum granulite.

White et al. (2004), the perthite–quartz assemblage in this figure is referred to as "in situ" leucosomes. Garnet$_1$ in this band contains ovoid inclusions of quartz (Fig. 5a) and fibrolitic sillimanite (sillimanite$_1$). The latter also occurs as rare prismatic grains in the matrix. Biotite is secondary and replaces garnet$_1$ along the perthite–garnet$_1$ grain boundary.

In the Larsara outcrop, in contrast, leucosomes occur as ~5 to 10 mm thick stringers, alternating with the melanocratic layers. On the basis of the mineral assemblage, two types of leucosomes are recognized: (1) quartz-bearing (quartz ≫ perthites), but devoid of porpyroblastic garnet$_1$ and (2) quartz-absent, perthite-rich leucosomes, containing garnet$_1$ ($Prp_{41}Grs_{03}Alm_{55}Sps_{01}$)–rutile–sillimanite–biotite assemblage, where rutile–sillimanite–biotite does not exceed by 5–10 vol.%. There are rare melanocratic micro-pods and lenses in the type 2 leucosome. Garnet$_1$ largely occurs as isolated rafts in the perthite-rich matrix. Perthite is generally mesoperthitic, the pre-exsolution composition of which varies between $Or_{47}Ab_{47}An_6$ (inclusion within garnet$_1$) and $Or_{51}Ab_{43}An_6$ (matrix) (Bhowmik et al., 2005). Both the external and internal outlines of porphyroblastic garnet against matrix and included perthites respectively, are of amoeboid shape (Fig. 5b). In contrast to Pipariya sample, quartz and sillimanite inclusions are lacking from garnet$_1$ in type 2 leucosome. Biotite$_1$ (X_{Mg}=0.81) occurs as inclusions in garnet$_1$ and also in the matrix. Spinel$_1$ (X_{Mg}=0.25) occurs as extremely rare inclusions in mesoperthites of type 2 leucosomes (Fig. 5c). Coarse sillimanite$_1$ in the leucosome matrix is occasionally rimmed by rare K-feldspar–spinel$_1$ with spinel preferentially adjoining sillimanite in contact with K-feldspar (Fig. 5d). Garnet$_1$ is generally armoured by

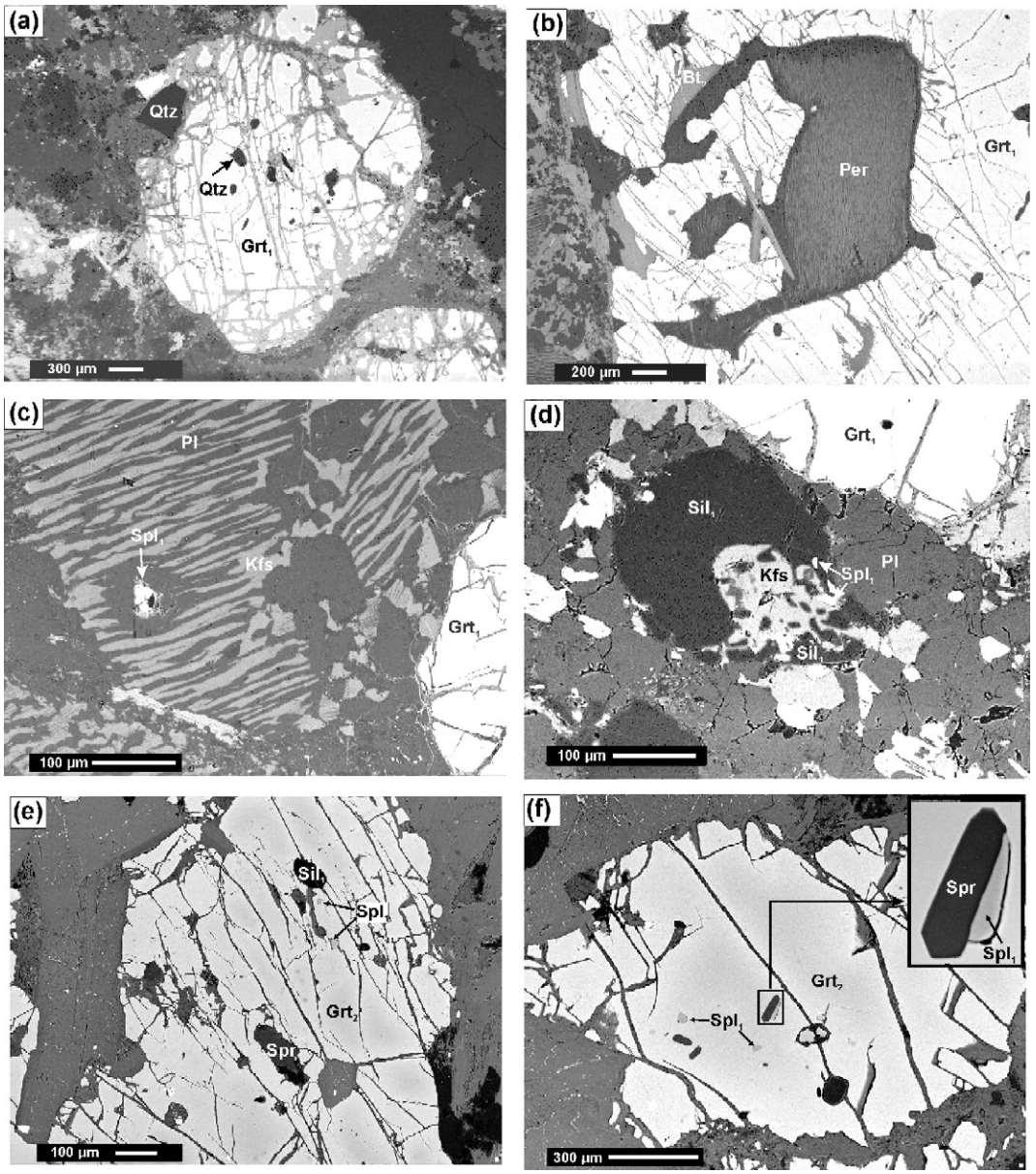

Fig. 5. Backscattered electron images, showing textures of different stages of ultrahigh-*T* metamorphism in the corundum granulite. (a) Porphyroblastic Grt (Grt_1) in sample B7B contains inclusions of Qtz. (b) Highly loabate to amoeboid internal margin of Grt_1 against included perthites (Per). (c) Inclusion of early generation Spl (Spl_1) within mesoperthites. (d) Matrix Sil (Sil_1) is rimmed by Kfs–Spl_1 assemblage. (e) Coarse coronal Grt_2 contains inclusion of Spr, Spl_1 and Sil_1. (f) Included Spr and Spl_1 in Grt_2 locally show straight grain boundary (shown in details in the inset).

retrograde $biotite_2 \pm sillimanite_2$ intergrowth in contact with perthites.

In the melanocratic band, quartz is totally absent. $Garnet_1$, perthites and plagioclase are minor minerals in this layer. Sapphirine ($X_{Mg}=0.73$), $spinel_1$ ($X_{Mg}=0.47$–0.52) and $sillimanite_1$ are always rimmed by a coarse variety of coronal garnet (Fig. 5e), designated as $garnet_2$ ($Prp_{38}Grs_{02}Alm_{59}Sps_{01}$). Included sapphirine and $spinel_1$ have rare grain contacts (Fig. 5f). Sapphirine and $spinel_1$ never occur in the matrix. $Garnet_2$ is generally found surrounding $garnet_1$. Idioblastic corundum, containing rare inclusions of $spinel_1$, is separated from $garnet_2$ by an intergrowth of $spinel_2$ ($X_{Mg}=0.31$–0.33)–$sillimanite_2 \pm biotite_2$ (Fig. 6e, f of Bhowmik et

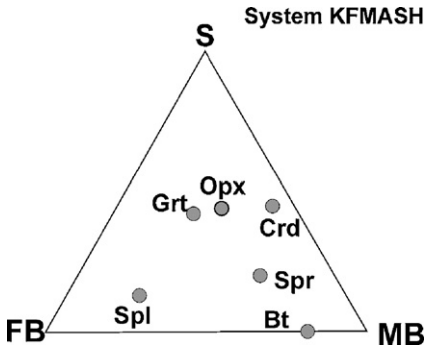

Fig. 6. Compositional relations between mineral phases in the S–FB–MB projection system for the corundum granulite.

al., 2005). In the latter case, spinel$_2$ is preferentially concentrated at the interface of corundum, while sillimanite$_2$ occurs around garnet. Biotite$_2$–spinel$_2$–sillimanite$_2$ symplectites occur as kelyphitic rims around garnet$_2$.

Bhowmik et al. (2005) interpreted the compositional relationship, $X_{Mg}(Spl_1) > X_{Mg}(Grt_2)$ for the melanocratic layers and, $X_{Mg}(Spl_1) < X_{Mg}(Grt_1)$ for the leucosomes to be due to Fe^{2+}–Mg exchange between co-existing garnet$_2$ and spinel$_1$, the extent of diffusion being largely controlled by the grain size of the exchanging phases. The authors predicted that the original spinel$_1$ was compositionally Fe-rich relative to that of garnet. Based on this compositional relationship, the X_{Mg} of the phases in the corundum granulites is considered to decrease in the following order: biotite–sapphirine–garnet–spinel. In the following section, using textural and compositional criteria, the sequence of mineral reactions in the studied rocks is established. For the latter, compositions of the co-existing phases in the aluminous granulites are plotted in the SiO_2–FB–MB ternary system (projected from sillimanite, K-feldspar, and melt) (Fig. 6), where FB and MB represent Fe- and Mg-rich biotite (after McDade and Harley, 2001). In addition, the chemograph also shows the projected orthopyroxene (composition from the associated felsic granulite (Anal No. B-3, sample no. B220A(1), after Bhowmik et al., 2005)) and cordierite compositions. This will be used to construct the KFMASH petrogenetic grid.

5. Mineralogical evolution

5.1. Prograde metamorphism

5.1.1. Corundum granulite

Field relations and textural features in the Pipariya outcrop reveal that initial melting in the aluminous protolith, leading to the stabilization of garnet$_1$ had taken place in quartz-bearing domain, following the generalized vapour-absent melting reaction,

$$\text{biotite}_1 + \text{sillimanite}_1 + \text{quartz} = \text{garnet}_1 + \text{perthite} + L \quad \text{(R1)}$$

Area calculation from in situ leucosomes containing garnet$_1$ (Fig. 4) when converted into molar proportions reveal Al/Si ratios at ~0.60, which is close to the Al/Si ratio in biotite (~0.49). This suggests bulk compositional control concerning the appearance of garnet$_1$ and leucosomes, both stabilized by the biotite-rich layer (also containing minor sillimanite) of the compositionally banded corundum granulite.

In contrast, in the Larsara exposure, the quartz-bearing type 1 leucosomes, being devoid of garnet$_1$ are segregated into mm-thick microbands, being separated from quartz-absent type 2 leucosomes by aluminous melanocratic layers. This raises the possibility of significant mobilization of the initial melts produced by reaction R1. During this process, the removal of silica would lead to silica-undersaturation in both the alumina-rich and alumina-poor intrabands.

In the next stage of mineralogical evolution, melting, initiated in the quartz-absent microdomains, due to a further rise in the temperature, led to the stabilization of the assemblage spinel$_1$–sapphirine. The preferential distribution of spinel$_1$–sapphirine in the melanocratic layers, surrounding garnet$_1$, the rare presence of spinel$_1$ within mesoperthites and the formation of K-feldspar–spinel$_1$ assemblage replacing sillimanite$_1$, suggest that this assemblage, in total absence of cordierite, quartz and orthopyroxene, could be produced by the KFMASH reaction:

$$\text{biotite}_1 + \text{garnet}_1 + \text{sillimanite}_1 \pm \text{K-feldspar} = \text{sapphirine} + \text{spinel}_1 + L \quad \text{(R2)}$$

The rare occurrence of sapphirine and spinel$_1$ in direct grain to grain contact (Fig. 5f) provides further support for the progress of reaction (R2). The amoeboid shape, of both the internal and external outlines of garnet$_1$ in contact with the included and the matrix mesoperthites, provides textural support for grain-scale re-equilibration of garnet$_1$ in the leucosomes during this stage of P–T evolution of the rock. During this process, the remaining biotite$_1$ and sillimanite$_1$ inclusions in garnet$_1$ after reaction (R1) could have completely disappeared. In the KFMASH system, reaction (R2), due to its steep dP/dT slope, progresses to the right with heating at temperature in

excess of 900 °C (McDade and Harley, 2001; Bhowmik et al., 2005). Because of the compositional relation, $X_{Mg}(Spl)<X_{Mg}(Grt)$, garnet and spinel in this reaction switch positions. This is in contrary to what has been shown in previous studies (e.g. Hensen and Harley, 1990; Mouri et al., 1996). Nevertheless, the sapphirine–spinel–sillimanite in the corundum granulites represents the peak metamorphic mineral assemblage in the BBG domain (Bhowmik et al., 2005).

5.1.2. Iron Formation granulite

In the Iron Formation granulite, textural evidence indicates that the type 1 pyroxenes stabilized during peak metamorphism. Reintegration of pyroxene exsolution textures also suggests that type 1 clinopyroxene appeared as ferroaugite (Fig. 3c). Metamorphic augite was previously reported from metamorphosed iron stones from Archaean Napier complex (Sandiford and Powell, 1986; Harley, 1987) and provides reliable evidence for UHT metamorphism (Harley, 1998a).

5.2. Retrograde metamorphism

5.2.1. Corundum granulite

Subsequent to the elimination of biotite$_1$ via reaction (R2), there were localized concentrations of sapphirine, spinel$_1$ and sillimanite$_1$ in the melanocratic layers, which led to its physical isolation from melt and K-feldspar-bearing compositional domains. This resulted in a shift of bulk composition from the larger KFMASH to the smaller FMAS system, for the next stage of mineralogical evolution. Inclusions of sapphirine, sillimanite$_1$ and spinel$_1$ in garnet$_2$ (Fig. 5e–f), the appearance of corundum containing inclusions of spinel$_1$, and the chemographic relationships (Fig. 6) suggest the simplified reaction:

$$\text{sapphirine} + \text{sillimanite}_1 + \text{spinel}_1 = \text{garnet}_2 + \text{corundum} \quad \text{(R3)}$$

This univariant reaction in the system FMAS is valid only if $X_{Mg}(Spl)<X_{Mg}(Grt)$. Reaction (R3) progresses to the right with cooling and/or increasing pressure. This suggests further silica undersaturation (Bhowmik et al., 2005). The rocks in this study, therefore, provide an evolutionary link between silica-saturated and silica-undersaturated rocks, which has been primarily brought about by the melting and removal of silica (McDade and Harley, 2001).

Development of a coarse symplectite, consisting of spinel$_2$–sillimanite$_2$–biotite$_2$ between garnet$_2$ and corundum in the melanocratic layer is due to the simplified reaction:

$$\text{garnet}_2 + \text{corundum} + L = \text{spinel}_2 + \text{sillimanite}_2 + \text{biotite}_2 \pm \text{K-feldspar} \quad \text{(R4)}$$

In the type 2 leucosomes, garnet$_1$, in contact with perthite, is also rimmed by coarse biotite$_2$–sillimanite$_2$ symplectites, which reflects the following generalized reaction,

$$\text{garnet}_1 + \text{perthites} + L = \text{biotite}_2 + \text{sillimanite}_2 \quad \text{(R5)}$$

Such melt–solid back reactions are commonly encountered during retrogression of UHT mineral assemblages (Moraes et al., 2002), where the melt provides the water necessary to stabilize biotite.

Extensive exsolution in alkali feldspar in the aluminous granulites, resulting in mesoperthite can be correlated with this cooling event.

5.2.2. Iron Formation granulite

In the Iron Formation granulite, there were multistage exsolutions involving type 1 pyroxenes at this stage. The following stages of exsolutions are recognized:

Stage 1

$$\text{ferroaugite} = \text{orthopyroxene}_1(\text{lamellae}) + \text{augite(host)} \quad \text{(R6)}$$

Stage 2

$$\text{orthopyroxene}_1 = \text{clinopyroxene(lamellae)} + \text{orthopyroxene(host)} \quad \text{(R7a)}$$

$$\text{augite host} = \text{orthopyroxene}_2(\text{lamellae}) + \text{clinopyroxene(host)} \quad \text{(R7b)}$$

Exsolutions of these types were previously recognized from augites of metamorphosed ironstones of the Napier complex, Antarctica (Sandiford and Powell, 1986; Harley, 1987) and are taken as evidence for slow cooling from extreme metamorphic temperatures ($T \geq 950$–1000 °C).

The formation of garnet as (i) lamellae, replacing orthopyroxene and augite lamellae formed by reaction (R7a) and (ii) layered garnet–quartz corona replacing

clinopyroxene against matrix plagioclase suggests that garnet could have appeared at the final stages of the exsolution process. For the coronal garnet, the following generalized garnet forming reaction is predicted,

clinopyroxene + plagioclase
= garnet + quartz (R8a)

The alumina required for the formation of lamellar garnet could be derived from the aluminous clinopyroxene host (Al_2O_3=2.56 wt.%) and the orthopyroxene lamellae, according to a generalized reaction of the type,

clinopyroxene + CaTs in Cpx + Opx + MgTs in Opx
= garnet (R8b)

Reaction (R8a) is generally modeled in terms of cooling, increasing pressure or both (Harley, 1989). In this study, reactions ((R7a), (R7b), (R8a) and (R8b)), when considered together give robust evidence for post-peak cooling.

The sequence of mineral reactions in these rocks is, therefore, the product of (a) heating, leading to partial melting in the aluminous granulites and stabilization of ferroaugites in the Iron Formation granulites (metamorphism BM_1) and (b) subsequent cooling (metamorphism BM_2), producing various types of coronas/symplectites and exsolution lamellae. The *P–T* conditions for peak and retrograde metamorphism are calculated in the following section using suitable thermobarometry calculations.

6. *P–T* conditions of metamorphism

Bhowmik et al. (2005) previously estimated *P–T* conditions of ~9 kbar, 950 °C for the peak BM_1 metamorphism and post-peak cooling to ~700 °C (BM_2). However, there is no reliable pressure estimate for the cooling event. In the present work, the *P–T* conditions during BM_2 are estimated using the garnet–clinopyroxene–orthopyroxene–plagioclase–quartz assemblage in the Iron Formation granulite. Additionally, the pyroxene quadrilateral thermometry (after Lindsley, 1983) is applied to estimate the peak metamorphic temperatures as well as the post-peak cooling. In the case of the latter, the thermodynamically corrected pre-exsolution compositions for ferroaugite ($Wo_{34}En_{32}Fs_{34}$) and the composition of co-existing orthopyroxene$_2$ ($Wo_{02}En_{36}Fs_{62}$) lamellae and the clinopyroxene ($Wo_{42}En_{31}Fs_{27}$) host are plotted in the pyroxene quadrilateral at *P* ~ 9 kbar (Fig. 3c). The stability of ferroaugite indicates a minimum temperature of ~1000 °C (Fig. 3c) for the BM_1 metamorphism, which is 50 °C higher than that estimated previously (Bhowmik et al., 2005). The tie line connecting co-existing orthopyroxene lamellae and clinopyroxene host suggests final exsolution at temperatures ~700 °C (Fig. 3c).

For the formation of coronal garnet, the Fe- and Mg-end member garnet–clinopyroxene–plagioclase–quartz geobarometers and a garnet–clinopyroxene geothermometer are used. These equilibria are calculated using the TWQ software (v.2.02) of Berman (1991). The three equilibria intersect at *P–T* conditions of ~9.5 kbar, 800 °C, if all Fe is taken as Fe^{2+} (Fig. 7). If Fe^{3+} is considered, calculated *P–T* change to ~8.3 kbar, 760 °C (Fig. 7). For the formation of lamellar garnet, temperature is calculated using garnet–orthopyroxene and garnet–clinopyroxene thermometers, which yield an average temperature of 670 °C at ~9 kbar (Fig. 7). The lower temperatures may indicate substantial retrograde Fe^{2+}–Mg exchange. Because of smaller volume of lamellar garnet, relative to pyroxenes, the garnet became more ferroan compared to coronal garnet. Based on these results, the *P–T* conditions during BM_2 are constrained at ~9.0 kbar, 700–750 °C.

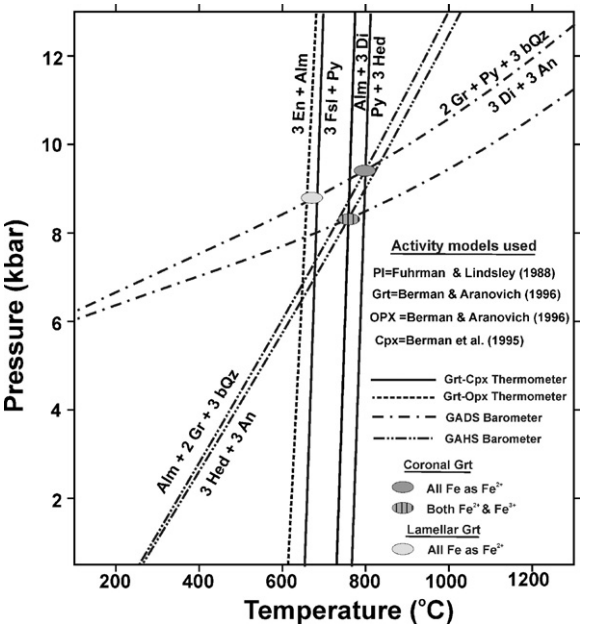

Fig. 7. The *P–T* conditions for retrograde metamorphism using Grt–Cpx–Opx–Pl–Qtz thermobarometry from the Iron Formation granulite. The activity models of minerals and the methodologies used for geothermobarometry are shown in the lower right part. Abbreviations used: GADS: garnet–anorthite–diopside–silica; GAHS: garnet–anorthite–hedenbergite–silica. Activity models used: PI=Fuhrman and Lindsley (1988); Grt=Berman and Aranovich (1996); OPX=Berman and Aranovich (1996); Cpx=Berman et al. (1995).

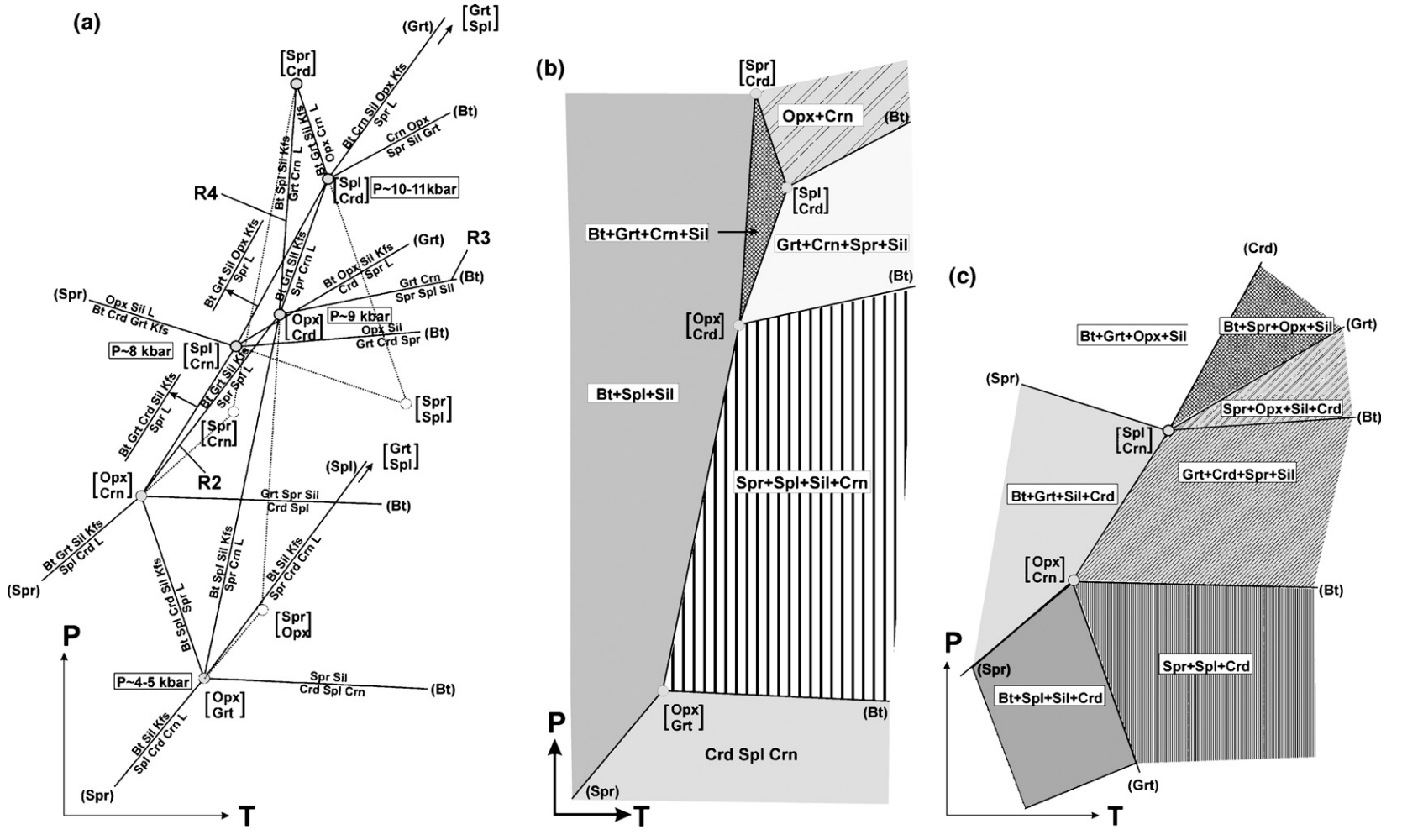

Fig. 8. (a) Qualitative KFMASH petrogenetic grid for corundum-bearing and corundum-absent aluminous granulites. (b–c) Mineral assemblage subfacies for corundum granulites (b) and corundum-absent aluminous granulites (c).

7. Petrogenetic grid

The mineralogical evolution of the corundum granulites during metamorphism can now be evaluated in terms of a suitable KFMASH petrogenetic grid. Although, analysis of corundum-bearing phase assemblages in the same system was previously made by Hensen and Harley (1990), Srogi et al. (1993), Sengupta et al. (1999) and Ouzegane et al. (2003), a petrogenetic grid in and around the [Opx, Crd] invariant point and involving the extremely rare sapphirine–spinel–sillimanite–garnet–corundum–biotite–K-feldspar mineral assemblage is presently lacking. Besides, the grid of Hensen and Harley (1990) was constructed based on the compositional relation of X_{Mg}(Spl)>X_{Mg}(Grt), which is the reverse in the present study. Existing KFMASH grids (e.g. Sengupta et al., 1999; McDade and Harley, 2001) also do not allow complete treatment of the corundum-bearing phase relations, particularly in UHT metamorphic conditions, as in the present study.

Notwithstanding the absence of experimental constraints on the melt composition, phase relations in the silica-undersaturated and high-alumina bulk composition as well as uncertainties associated with entropy and a–X relationships for sapphirine, recent progress in treating KFMASH phase relations (excluding corundum) in the same bulk composition (e.g. McDade and Harley, 2001), provides a useful basis for including corundum in the KFMASH phase relations. In particular, the grid of McDade and Harley (2001) allows the silica-undersaturated part of phase relations to be studied via two critical invariant points, [Opx, Qtz] and [Spl, Qtz]. In aluminous granulites, these quartz-absent invariant points connect the lower and higher temperature silica-oversaturated part of the system by assuming that silica undersaturation in aluminous bulk rock composition may be a natural consequence of melt generation by biotite-melting and subsequent melt extraction from the site of melting. The grid of McDade and Harley (2001) predicts that quartz-absent invariant points may stabilize at metamorphic temperatures in excess of KFMASH [Opx,Spr] and [Spr,Spl] invariant points. In the aluminous granulites of the present study, the bulk of mineralogical evolution took place in quartz-absent domains. Therefore, by drawing analogy with previous studies, which allowed quartz-absent invariant points to coincide with corundum-absent ones (Hensen, 1987), [Opx, Qtz] and [Spl, Qtz] points in the present grid are renamed as [Opx, Crn] and [Spl, Crn], respectively (Fig. 8a). Assuming that these points are stable and allow connection with corundum-bearing paragenesis, a qualitative KFMASH petrogenetic grid has been constructed following the approach and methodology of McDade and Harley (2001) and with the same caveats as explained by the authors.

In the 6-component, 10 phase KFMASH system of biotite (Bt), sillimanite (Sil), K-feldspar (Kfs), spinel (Spl), garnet (Grt), sapphirine (Spr), corundum (Crn), orthopyroxene (Opx), cordierite (Crd) and melt (L), the following compositional relationship of X_{Mg}(Spl)<X_{Mg}(Grt)<X_{Mg} (Opx)<X_{Mg}(Spr)<X_{Mg}(Bt)<X_{Mg}(Crd) has been followed. From Fig. 6, the balanced univariant reactions around the selected invariant points are shown in Table 3. The petrogenetic grid is shown in Fig. 8a. As noted in previous studies (e.g. Harley and Motoyoshi, 2000; McDade and Harley, 2001; Ouzegane et al., 2003), the slopes of sapphirine-bearing reactions are affected by the assumed entropy of sapphirine. In this work, 793 Fe- and Mg-end member sapphirines, (where the number refers to molar (Mg,Fe)O: Al_2O_3:SiO_2 ratio) have been used so that the sapphirine-bearing mineral assemblages are stable at high temperatures and orthopyroxene–corundum-bearing ones are stable on the high pressure side of the univariant reactions. Negligible amount of calculated Fe^{3+}, both in spinel and sapphirine, together with the presence of rutile imply low fO_2 metamorphic conditions. Although, spinel contains moderate amounts of gahnite, the total non-FMAS contents do not exceed 10 mol%. This suggests that the phase relations in the corundum granulites can be reasonably interpreted using the new grid.

Apart from [Opx, Crn] and [Spl, Crn] invariant points of the previously suggested petrogenetic grid, the new grid considers the stability of [Opx, Crd] based on three univariant reactions ((R2), (R3) and (R4)). The invariant point is positioned up pressure on the univariant reaction (Opx, Crn, Crd) (reaction (R2)) and at a pressure higher than that of [Spl, Crn] invariant point. This is inferred based on the silica undersaturated FMAS grid of Hensen (1987), which predicts that the FMAS (Crd, Opx) univariant reaction is positioned at a higher pressure relative to that of FMAS (Spl, Crn) reaction. In this grid, the (Bt) absent reaction is also considered to be (Kfs, L) absent (see McDade and Harley, 2001 for an alternative assumption) and that the (Opx, Crd, Bt) and (Spl, Crn, Bt) reactions are equivalent to FMAS (Crd, Opx) and (Spl, Crn) reactions. Because of the relatively flat slopes of these reactions, the assumed location of the [Opx, Crd] vis-à-vis [Spl, Crn] invariant points seems justified. The relatively higher pressure stability of the [Opx, Crd] invariant point is also indicated by an independent P–T estimate of ~9 kbar, 950°–1000 °C (Bhowmik et al., 2005 and this study). Schreinemaker's analysis around

the [Opx, Crd] invariant point results in three additional invariant points, namely [Spl, Crd], [Grt, Opx] and [Spr, Crd] (Fig. 8a), which are consistent with the natural rock data. The justification of the lower pressure [Opx, Grt] invariant point, which results from the intersection of the univariant reactions (Opx, Crd, Grt) and (Opx, Crn, Grt) comes from several studies in shallow contact aureoles (Grant, 1985; Pattison and Harte, 1985; Grant and Frost, 1990; Pattison and Harte, 1991), as well as in low-*P*, high-*T* regional metamorphic terrain of Namaqualand (Waters, 1986). In the aureoles, low-pressure heating (at $P \sim 3$ kbar) has intersected several equilibria emanating from the [Grt, Opx] and the [Opx, Crn] invariant points. In the Laramie aureole, the reaction (Grt, Opx, Spr), which emanates from the [Grt, Opx] invariant point towards its lower pressure end provides a pressure constraint of 3 kbar $< P_{[\mathrm{Grt,\ Opx}]} < P_{[\mathrm{Opx,Crn}]}$. Waters (1986) has established that the reaction (Grt, Opx, Bt) occurs in the Namaqualand metamorphic belt. Pressures of ~5 kbar were estimated for metamorphism in the vicinity of [Grt, Opx, Bt] point. The [Spl, Crd] invariant point, which results from the intersection of the (Spl, Crn, Crd) and (Opx, Crd, Spl) univariant reactions, occurs at pressures higher than that of the [Opx, Crd] invariant point (Ouzegane et al., 2003; Kelly and Harley, 2004). These workers have shown that the orthopyroxene–corundum assemblage is stable at $P \sim 10$–11 kbar and at temperatures of ~850°–900 °C as well as a number of FMAS divariant reactions in and around the [Spl, Crd, Bt] invariant point. These reactions were intersected in response to near isothermal decompression, producing a sequence of mineral assemblages, which are consistent with the present grid. The grid also predicts that the rare [Spr, Crd] invariant point is stable at the highest pressure.

Using the grid in Fig. 8a, two separate phase relations are constructed, one for the corundum granulites (Fig. 8b) and the other for corundum-absent, silica undersaturated metapelite granulites (Fig. 8c). The grid for the corundum granulite differs from previous KFMASH grids (e.g. Hensen and Harley, 1990; Sengupta et al., 1999; McDade and Harley, 2001) in several aspects, namely: (1) the [Spr, Spl] and also the [Spr, Opx] invariant points, which were considered as stable in all previous grids, are metastable in the present grid. The [Opx, Crd] invariant point, which is metastable in those previous studies of the KFMASH grid, owes its stability in this study, possibly because of the relatively Fe-rich bulk composition of the corundum granulites. (2) The KFMASH grid predicts that corundum can appear in silica-undersaturated metapelites both as a product of biotite melting and solid–solid reactions. In particular, the grid shows that the sapphirine–corundum assemblage can be a reliable indicator for UHT metamorphism. (3) One of the

Table 3
Balanced univariant reactions in KFMASH system

[Opx, Crd]
(Crn) 0.0198Bt+0.0154Grt+0.1366Sil+0.0111Kfs=0.0667Spr+0.0101Spl+0.37*L*
(Spr) 0.0198Bt+0.2028Spl+0.4155Sil+0.0111Kfs=0.0961Grt+0.5256Crn+0.37*L*
(Spl) 0.0198Bt+0.0101Grt+0.1498Sil+0.0111Kfs=0.025Crn+0.0636Spr+0.37*L*
(Bt) 0.2121Grt+1Crn=0.127Spr+0.4051Spl+0.5308Sil
(Grt) 0.0198Bt+0.0193Spl+0.1751Sil+0.0111Kfs=0.0575Spr+0.0726Crn+0.37*L*

[Spl, Crd]
(Crn) 0.0198Bt+0.0071Grt+0.142Sil+0.0111Kfs+0.012 Opx=0.0711Spr+0.37*L*
(Spr) 0.0198Bt+0.2128Sil+0.0356Grt+0.0111Kfs=0.1034Opx+0.2372Crn+0.37*L*
(Opx) 0.0198Bt+0.0101Grt+0.1498Sil+0.0111Kfs=0.025Crn+0.0636Spr+0.37*L*
(Bt) 0.247Grt+0.6068Sil+0.6148Spr=2.0528Crn+1Opx
(Grt) 0.0198Bt+0.059Crn+0.1249Sil+0.0409Opx+0.0111Kfs=0.0887Spr+0.37*L*

[Spl, Crn]
(Crd) 0.0198Bt+0.0071Grt+0.142Sil+0.0111Kfs+0.012 Opx=0.0711Spr+0.37*L*
(Spr) 0.0198Bt+0.6686Crd+0.7227Grt+0.0111Kfs=1.9304Opx+1.7929Sil+0.37*L*
(Opx) 0.0198Bt+0.0116Grt+0.0042Crd+0.1303Sil+0.0111Kfs=0.0706Spr+0.37*L*
(Bt) 0.3698Grt+0.3454Crd+0.0367Spr=1.0038Opx+1Sil
(Grt) 0.0198Bt+0.1616Sil+0.0314Opx+0.0111Kfs=0.0066Crd+0.0717Spr+0.37*L*

[Opx, Crn]
(Crd) 0.0198Bt+0.0154Grt+0.1366Sil+0.0111Kfs=0.0667Spr+0.0101Spl+0.37*L*
(Spr) 0.0198Bt+0.0814Grt+0.2449Sil+0.0111Kfs=0.1849Spl+0.0723Crd+0.37*L*
(Spl) 0.0198Bt+0.0116Grt+0.0042Crd+0.1303Sil+0.0111Kfs=0.0706Spr+0.37*L*
(Bt) 0.989Grt+1.6229Sil+1Spr=1.084Crd+2.619Spl
(Grt) 0.0198Bt+0.0307Spl+0.1113Sil+0.0169Crd+0.0111Kfs=0.0823Spr+0.37*L*

[Opx, Grt]
(Crd) 0.0198Bt+0.0193Spl+0.1751Sil+0.0111Kfs=0.0575Spr+0.0726Crn+0.37*L*
(Spr) 0.0198Bt+0.3232Sil+0.0111Kfs=0.0391Crd+0.0071Spl+0.2411Crn+0.37*L*
(Spl) 0.0198Bt+0.2834Sil+0.0111Kfs=0.0154Spr+0.0286Crd+0.1958Crn+0.37*L*
(Bt) 0.2323Crd+0.1565Spl+1Crn=0.8788Sil+0.3414Spr
(Crn) 0.0198Bt+0.0307Spl+0.1113Sil+0.0169Crd+0.0111Kfs=0.0823Spr+0.37*L*

important outcomes of the new KFMASH grid is that it enables the delineation of different corundum-bearing mineral assemblages, each having distinct stability limits in P–T space (Fig. 8b). Of particular interest is the recognition of four pressure zones at ultra high temperatures (Fig. 8b). From lower to higher pressures, these zones are: (1) spinel–cordierite–corundum, (2) sapphirine–spinel–sillimanite, (3) garnet–corundum and (4) orthopyroxene–corundum. Although the utility of the spinel–cordierite–corundum, garnet–corundum (Sengupta et al., 1999) and orthopyroxene–corundum (Kelly and Harley, 2004) as depth markers have been previously predicted from partial KFMASH and FMASH petrogenetic grid studies, the new grid first links these different metamorphic subfacies, thereby enhancing its general applicability in different metamorphic terrains. Additionally, this grid identifies the sapphirine–spinel–sillimanite sub-assemblage as distinct marker for ultra high temperature metamorphism at intermediate-deeper crustal levels. The occurrence of garnet–corundum as a distinct high pressure assemblage ($P>9$ kbar) (e.g. Fig. 8a, reaction (R3)) in silica undersaturated metapelites is quite significant and can be taken as a diagnostic for high pressure metamorphism in the same light as orthopyroxene–sillimanite–quartz is considered for silica oversaturated metapelites. At still higher pressures, garnet–corundum is replaced by orthopyroxene–corundum. For the corundum-absent, silica undersaturated metapelite granulites, the delineation of five pressure zones: sapphirine–cordierite–spinel, garnet–cordierite–sapphirine–sillimanite, sapphirine–orthopyroxene–sillimanite–cordierite, biotite–sapphirine–orthopyroxene–sillimanite and biotite–garnet–orthopyroxene–sillimanite from low to high pressure (Fig. 8c) is consistent with natural rock data (Harley, 1986, 1998b; Baba, 2003; Sajeev et al., 2004).

8. Metamorphic P–T path and tectonic significance of UHT granulites in the CITZ

The methodologies and approaches followed in the present study demonstrate that corundum granulites can be profitably used to accurately constrain the metamorphic P–T path of UHT terranes. In the BBG domain, at the southern margin of the Central Indian Tectonic Zone, these rocks preserve a multistage metamorphic reaction history, resulting in the following sequence of mineral assemblages: porphyroblastic garnet$_1$, (reaction (R1)), sapphirine–spinel$_1$–rutile (reaction (R2)), coronal garnet$_2$–corundum (reaction (R3)) and, finally, biotite$_2$–sillimanite$_2$–spinel$_2$ (reaction (R4)). When considered in the newly constructed KFMASH petrogenetic grid, these reactions reveal a prograde segment (R2) at pressures below the [Crd, Opx] invariant point, culminating in the peak metamorphic conditions of ~1000 °C, 9 kbar (BM_1), a pressure increase (R3) and finally a near isobaric cooling (R4) of ~250–300 °C (BM_2) at $P>P_{[Crd,Opx]}$. The textural development at each stage of metamorphic evolution is shown with the help of cartoon sketches in Fig. 9. The deduced metamorphic P–T path has a counterclockwise sense (Fig. 9). Considering that near isobaric cooling from T_{Max} is a natural consequence of thermal relaxation of the perturbed geotherm, the BM_1–BM_2 metamorphic stages can be considered to belong to the same UHT metamorphic event. The close spatial association of the metagabbros with the UHT granulites (in ~1:1 volume ratio in the exposure scale) also suggests that the thermal perturbation necessary to cause the extreme temperatures was provided by intraplated basaltic magmas. In the majority of studies of UHT terrains, the counterclockwise P–T path is deduced on the basis of deep crustal heating–cooling P–T trajectory (Waters, 1989; Dasgupta et al., 1997; Sengupta et al., 1999). The increase in pressures, as demonstrated in the present study using the KFMASH grid, is, therefore, extremely significant and may suggest magmatic overplating in the BBG crust. Based on electron microprobe dating techniques on monazites, Bhowmik et al. (2005) suggested a Palaeoproterozoic age (~2040–2090 Ma) for this UHT metamorphism.

Previous tectonic models proposed a major Palaeoproterozoic collisional orogeny in the CITZ, leading to the amalgamation of the North and the South Indian Blocks along the Central Indian Suture (cf. CIS) (Yedekar et al., 1990; Jain et al., 1991, 1995; Mishra et al., 2000). These models were based on the following lithological, geochemical and geophysical arguments: (1) rocks of contrasting modes of occurrence, mineral assemblages and metamorphic grades occur across the CIS, with low-grade volcanogenic sequences lying to the south and the high-grade metasediments and granulites occurring to its north. (2) Calc-alkaline geochemical signatures in the Dongargarh granitoids, Dongargarh and Sakoli volcanics were taken as evidence for subduction-related magmatism, as a sequel to this suturing event. (3) The granulites of the BBG domain were interpreted as the exhumed oceanic crust of the North Indian Block that was subducted below the South Indian Block during this collision orogeny. (4) Seismic profile and gravity modeling studies show a sharp variation in the crustal thickness and gravity anomaly across the CIS.

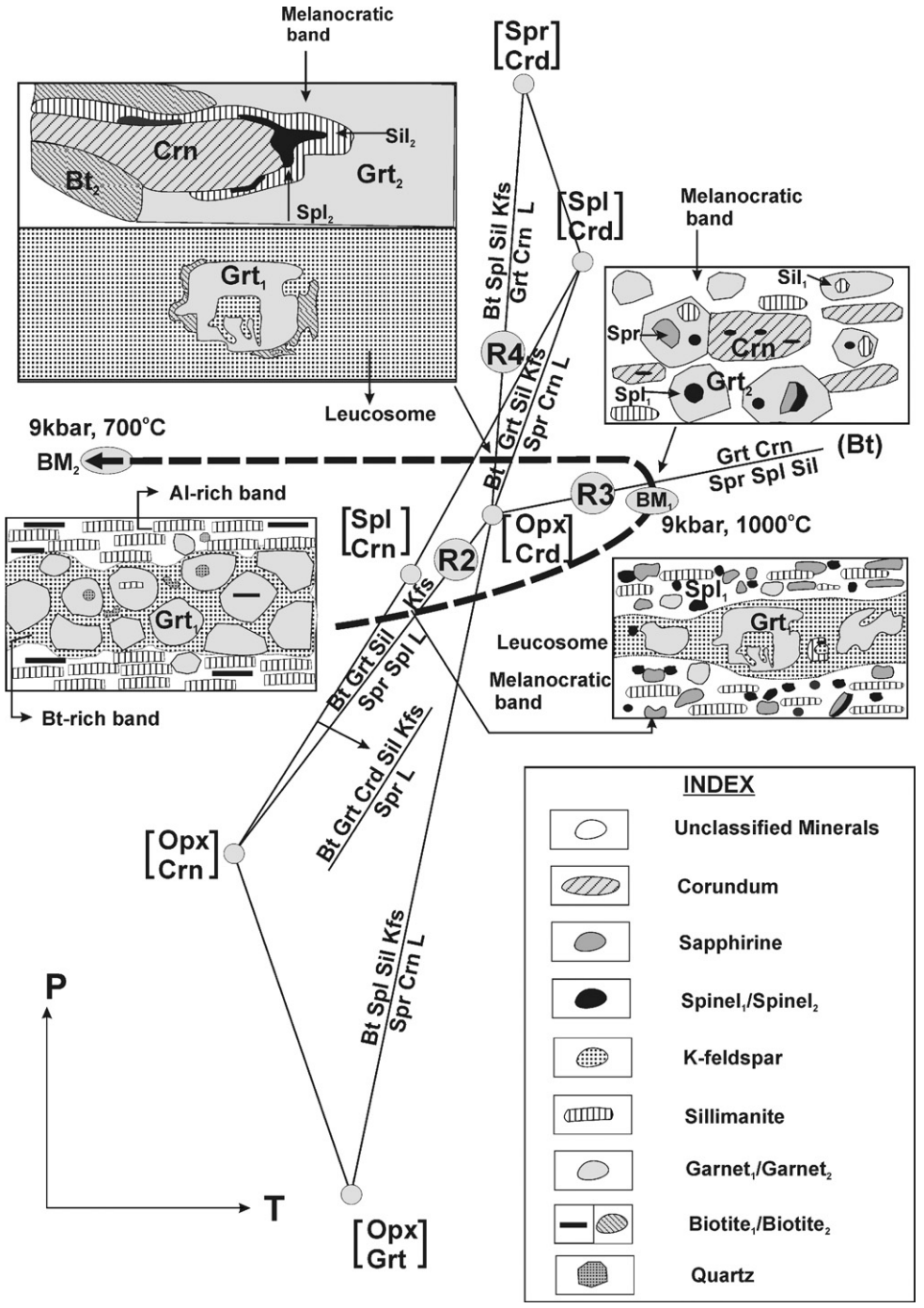

Fig. 9. Schematic representation of the mineral textural development in corundum granulites along a counterclockwise *P–T* path superimposed on a qualitative KFMASH petrogenetic grid.

Recent metamorphic and geochronological studies across the Sausar Mobile Belt provide new insight into the crustal evolutionary processes that were operative in the CITZ (Bhowmik and Roy, 2003; Bhowmik and Spiering, 2004; Bhowmik et al., 2005) and contradict simple, single-cycle plate convergence model of the previous workers. Firstly, in contrast to the simple low- and high-grade contrast across the CIS, it has been shown that the high-grade rocks of the BBG domain occur as allochthonous tectonic slices, being bounded

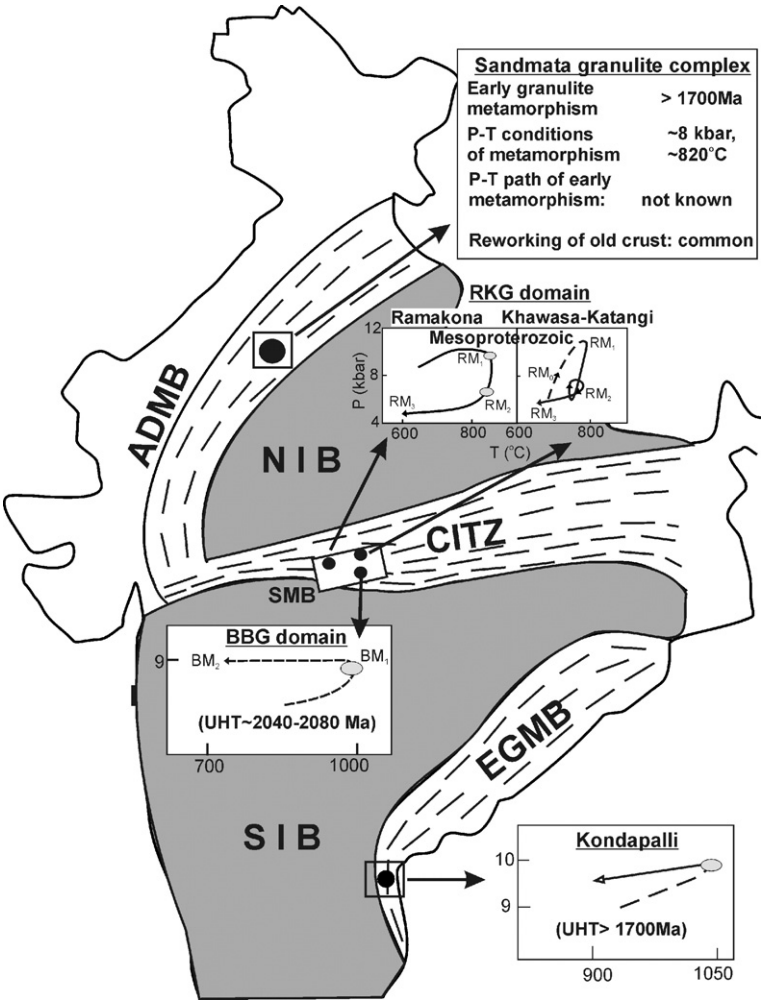

Fig. 10. Contrasting metamorphic *P–T* paths, related to temporally separate metamorphic events from two spatially associated metamorphic domains in the Sausar Mobile Belt, at the southern margin of the Central Indian Tectonic Zone (CITZ). This possibly signifies the presence of amalgamated crust in the CITZ. The figure also shows correlation of Palaeoproterozoic metamorphic events in the mobile belts of Peninsular India.

on both sides by low-grade rocks (Bhowmik and Pal, 2000; Bhowmik et al., 2005). Secondly, the Dongargarh granitoids and the Dongargarh and Sakoli volcanics of Palaeoproterozoic age (Sarkar et al., 1981) have a distinct N–S structural orientation, paralleling the structural grain of the SIB, but discordant to the E–W to ENE–WSW trending CITZ. Had these rocks been produced during north–south compressional orogeny, stitching the two cratonic blocks, the rocks would have a broad E–W to ENE–WSW alignment, paralleling the orientation of the CITZ. Consequently, the calc-alkaline signatures of these rocks as well as their Palaeoproterozoic ages cannot be incorporated into tectonic models of the amalgamation of the two crustal blocks. Thirdly, the mafic–ultramafic components of the BBG domain are predominantly concordant gabbroic, noritic and orthopyroxenite intrusive bodies within the supracrustal granulite ensemble. The gabbroic intrusions are interpreted as intraplate mafic intrusions, synchronous with the Palaeoproterozoic UHT metamorphism (Bhowmik et al., 2005 and this study), and cannot be taken as evidence for the subducted oceanic crust. In contrast, the counterclockwise sense of the *P–T* path, pigeonholed from this domain, argues against collisional orogeny in the CITZ during the Palaeoproterozoic. Instead, such ultrahigh temperature metamorphism and a counterclockwise *P–T* path possibly suggest cratonization (stabilization through isobaric cooling) of the CITZ in the Palaeoproterozoic.

Recent studies established a regional high-pressure metamorphic belt with a clockwise metamorphic *P–T* path from the Ramakona–Katangi granulite domain, at

Table 4

Proterozoic Mobile Belts	Eastern Ghats Mobile Belt	Central Indian Tectonic Zone	Aravalli Delhi Mobile Belt
A. Location	Kondapalle granulites	BBG domain (this study)	Sandmata granulite complex
B. Tectonic framework	Granulite complex on the shoulders of Eastern Dharwar craton	Granulite complex on the northern margin of the South Indian Block	Granulite complex as pods and lenses within the Archaean Banded Gneissic Complex (?)
C. Tectono-magmatic and tectonothermal stratigraphy	Formation of protoliths for Crn granulite-calc silicate granulite-khondalite	Formation of protoliths for Crn granulite–felsic granulite–Iron Formation granulite–grt–crd granulite	Formation of protoliths for khondalite-calc silicate granulite–leptynitic gneiss
	Emplacement of mafic layered intrusion of gabbronorite–pyroxenite–anothosite	Emplacement of mafic layered intrusion of gabbro–noritic gabbro	Emplacement of mafic intrusion of gabbro
	Attendant UHT metamorphism, leading to partial melting in pelites and segregation of leucocratic and melanocratic layers	Attendant UHT metamorphism, producing partial melting in pelites and segregation of leucocratic and melanocratic layers	Attendant granulite metamorphism, partial melting in pelites and segregation of leucocratic and melanocratic layers
	Enderbite–charnoenderbite plutonism (c.1700–1720 Ma) post-dating UHT		Megacrystic charnockite–enderbite–granodiorite (c.1723 Ma) plutonism post-dating granulite metamorphism
	Emplacement of noritic dyke	Emplacement of gabbronorite dykes	Emplacement of norite dykes
	Emplacement of doleritic dyke		
	Emplacement of allanite-bearing granitic pegmatite (U–Pb cooling ages of allanite and monazite in the range ~1600–1672 Ma)		
D. Metamorphism			
P–T conditions of metamorphism	$P>\sim 8$ kbar, $T>\sim 1000$ °C	$P\sim 9$ kbar, $T\sim 1000$ °C	$P\sim 8$ kbar, $T\sim 820$ °C
P–T path	CCW	CCW	Not known
Age of metamorphism	>1720 Ma	~2040–2080 Ma	>1723 Ma
E. Tectonic set up	Palaeoproterozoic continental rifting (?)	Palaeoproterozoic continental rifting (?)	Palaeoproterozoic continental rifting (?)

Source of data: EGMB, Sengupta et al. (1999), Mezger and Cosca (1999), Kovach et al. (2001); CITZ, Bhowmik and Dasgupta (2004), Bhowmik et al. (2005) and this study; ADMB, Sarkar et al. (1989); Dasgupta et al. (1995), Bhowmik and Dasgupta (2004).

the northern margin of the Sausar Mobile Belt (Bhowmik and Roy, 2003; Bhowmik and Spiering, 2004). These studies reveal an early continental subduction followed by continent–continent collision event, leading to the final amalgamation of the North and South Indian Blocks. Available geochronological data indicates that the collisional orogeny is of Mesoproterozoic age and distinctly younger than the Palaeoproterozoic UHT event (Bhowmik and Roy, 2003; Bhowmik and Dasgupta, 2004). The recognition of two spatially associated but temporally separate metamorphic domains, and recording contrasting tectonothermal history in the southern margin of the Central Indian Tectonic Zone (Fig. 10) is, therefore, extremely significant. These findings possibly imply presence of amalgamated crustal domains in this tectonic zone. The amalgamation between the North and the South Indian Blocks is likely to be of Mesoproterozoic age. Santosh et al. (2004) have also speculated a Mesoproterozoic terrane amalgamation from another crustal domain of the Central India.

Bhowmik and Dasgupta (2004) have recently noted remarkable similarities in the tectono-magmatic, tectono-metamorphic, metamorphic *P–T* paths and common mafic magmatism during the Palaeoproterozoic period in the mobile belts, straddling the Archaean cratonic blocks (Fig. 10) (summarized in Table 4). These findings appear to justify previous correlations, which predicted uniform Mesoproterozoic and Meso-Neoproterozoic crustal evolutionary histories of the Eastern Ghats Mobile Belt, Central Indian Tectonic Zone and the Aravalli Delhi Mobile Belt

(Fig. 10) (Naqvi and Rogers, 1987). Additionally, the present study infers common Palaeoproterozoic histories in these belts also.

Acknowledgements

The research was funded by the Department of Science and Technology (Grant No. ESS/23/VES/129/2000) and the Indian National Science Academy-Deutsche Forschungsgemeinschaft research fellowship. Prof. M. Santosh and Dr. K. Sajeev are thanked for inviting me to write the paper. The paper has been benefited by the comments of Dr. A. Liati and Dr. D. Harlov and the competent editorial handling of Prof. M. Santosh. Discussions with Prof. S. Dasgupta and Prof. A. Bhattacharyya were of considerable help to improve the manuscript. A. Basu Sarbadhikari is also thanked for assistance at different stages of preparation of the manuscript.

References

Andersen, D.J., Lindsley, D.H., Davidson, P.M., 1993. QUILF: a PASCAL program to assess equilibria among Fe–Mg–Ti oxides, pyroxenes, olivine, and quartz. Comput. Geosci. 19, 1333–1350.

Baba, S., 2003. Two stages of sapphirine formation during prograde and retrograde metamorphism in the Palaeoproterozoic Lewisian Complex in South Harris, NW Scotland. J. Petrol. 44, 329–354.

Berman, R.G., 1991. Thermobarometry using multi-equilibrium calculations: a new technique, with petrological applications. Can. Mineral. 29, 833–855.

Berman, R.G., Aranovich, L.Y., 1996. Optimized standard state and solution properties of minerals: I. Model calibration for olivine, orthopyroxene, cordierite, garnet, and ilmenite in the system FeO–MgO–CaO–Al_2O_3–TiO_2–SiO_2. Contrib. Mineral. Petrol. 126, 1–24.

Berman, R.G., Aranovich, L.Y., Pattison, D.R.M., 1995. Reassessment of the garnet–clinopyroxene Fe–Mg exchange thermometer: II. Thermodynamic analysis. Contrib. Mineral. Petrol. 119, 30–42.

Bertrand, P., Ouzegane, Kh., Kienast, J.R., 1992. P–T–X relationships in the Precambrian Al–Mg-rich granulites from In Ouzzal, Hoggar, Algeria. J. Metamorph. Geol. 10, 17–31.

Bhowmik, S.K., Dasgupta, S., 2004. Tectonometamorphic evolution of boudin-type granulites in the Central Indian Tectonic Zone and in the Aravalli Delhi Mobile Belt: a synthesis and future perspectives. Special Publication Volume of the Geological Survey of India, vol. 84, pp. 227–246.

Bhowmik, S.K., Roy, A., 2003. Garnetiferous metabasites from the Sausar Mobile Belt: petrology, P–T path and implications for the tectonothermal evolution of the Central Indian Tectonic Zone. J. Petrol. 44, 387–420.

Bhowmik, S.K., Spiering, B., 2004. Constraining the prograde and retrograde *P–T* paths of granulites using decomposition of initially zoned garnets: an example from the Central Indian Tectonic Zone. Contrib. Mineral. Petrol. 147, 581–603.

Bhowmik, S.K., Pal, T., 2000. Petrotectonic implication of the granulite suite north of the Sausar mobile belt in the overall tectonothermal evolution of the Central Indian mobile belt. Geological Survey of India Unpublished Progress Report.

Bhowmik, S.K., Basu Sarbadhikari, A., Spiering, B., Raith, M.M., 2005. Mesoproterozoic reworking of Palaeoproterozoic ultrahigh temperature granulites in the Central Indian Tectonic Zone and its implications. J. Petrol. 46, 1085–1119.

Carrington, D.P., Harley, S.L., 1995. Partial melting and phase relations in high-grade metapelites: an experimental petrogenetic grid in the KFMASH system. Contrib. Mineral. Petrol. 120, 270–291.

Currie, K.L., Gittins, J., 1988. Contrasting sapphirine parageneses from Wilson Lake, Labrador and their tectonic implications. J. Metamorph. Geol. 6, 603–622.

Dasgupta, S., Sengupta, P., Ehl, J., Raith, M., Bardhan, S., 1995. Reaction textures in a suite of spinel granulites from the Eastern Ghats Belt, India: evidence for polymetamorphism, apartial petrogenetic grid in the system KFMASH and the roles of ZnO and Fe_2O_3. J. Petrol. 36, 435–461.

Dasgupta, S., Ehl, J., Raith, M.M., Sengupta, P., Sengupta, P., 1997. Deep crustal contact metamorphism around the Chimakurthy mafic–ultramafic Complex, Eastern Ghats Belt, India. Contrib. Mineral. Petrol. 129, 182–197.

Droop, G.T.R., 1989. Reaction history of garnet–sapphirine granulites and conditions of Archaean high-pressure granulite-facies metamorphism in the Central Limpopo Mobile Belt, Zimbabwe. J. Metamorph. Geol. 7, 383–403.

Ellis, D.J., Sheraton, J.W., England, R.N., Dallwitz, W.B., 1980. Osumilite–sapphirine–quartz granulites from Enderby Land, Antarctica: mineral assemblages and reactions. Contrib. Mineral. Petrol. 72, 123–143.

Eriksson, P.G., Mazumder, R., Sarkar, S., Bose, P.K., Altermann, W., van der Merwe, R., 1999. The 2.7–2.0 Ga volcano-sedimentary record of Africa, India and Australia: evidence for global and local changes in sea level and continental freeboard. Precambrian Res. 97, 269–302.

Fuhrman, M.L., Lindsley, D.H., 1988. Ternary-feldspar modeling and thermometry. Am. Mineral. 73, 201–215.

Goncalves, P., Nicollet, C., Montel, J.M., 2004. Petrology and in situ U–Th–Pb monazite geochronology of ultrahigh-temperature metamorphism from the Andriamena Mafic Unit, North-Central Madagascar. Significance of a petrographical *P–T* path in a polymetamorphic context. J. Petrol. 45, 1923–1957.

Grant, J.A., 1985. Phase equilibria in partial melting of pelitic rocks. In: Ashworth, J.R. (Ed.), Migmatites. Blackie and Son, Glasgow, pp. 86–144.

Grant, J.A., Frost, B.R., 1990. Contact metamorphism and partial melting of pelitic rocks in the aureole of the Laramie anorthosite complex, Morton Pass, Wyoming. Am. J. Sci. 290, 425–472.

Grew, E.S., 1982. Osumilite in the sapphirine–quartz terrane of Enderby Land, Antarctica: implications for osumilite petrogenesis in the granulite facies. Am. Mineral. 67, 762–787.

Harley, S.L., 1985. Garnet–orthopyroxene bearing granulites from Enderby Land, Antarctica: metamorphic pressure–temperature–time evolution of the Archaean Napier Complex. J. Petrol. 26, 819–856.

Harley, S.L., 1986. A sapphirine–cordierite–garnet–sillimanite granulite from Enderby Land, Antarctica: implications for FMAS petrogenetic grids in the granulite facies. Contrib. Mineral. Petrol. 94, 452–460.

Harley, S.L., 1987. A pyroxene-bearing metaironstone and other pyroxene-granulites from Tonagh Island, Enderby Land,

Antarctica: further evidence for very high temperature (>980 °C) Archaean regional metamorphism in the Napier Complex. J. Metamorph. Geol. 5, 341–356.

Harley, S.L., 1989. The origin of granulites: a metamorphic perspective. Geol. Mag. 126, 215–247.

Harley, S.L., 1998a. On the occurrence and characterisation of ultrahigh-temperature crustal metamorphism. In: Treloar, P.J., O'Brien, P.J. (Eds.), What Drives Metamorphism and Metamorphic Reactions? In: Geol. Soc. London, Spec. Publ., vol. 138, pp. 81–107.

Harley, S.L., 1998b. Ultrahigh temperature granulite metamorphism (1050 °C, 12 kbar) metamorphism and decompression in garnet (Mg-70)-orthopyroxene–sillimanite gneisses from the Rauer Group, East Antarctica. J. Metamorph. Geol. 16, 541–562.

Harley, S.L., 2004. Extending our understanding of ultrahigh temperature crustal metamorphism. J. Mineral. Petrol. Sci. 99, 140–158.

Harley, S.L., Motoyoshi, Y., 2000. Al zoning in orthopyroxene in a sapphirine quartzite: evidence for >1120 °C UHT metamorphism in the Napier Complex, Antarctica, and implications for the entropy of sapphirine. Contrib. Mineral. Petrol. 138, 293–307.

Harley, S.L., Hensen, B.J., Sheraton, J.W., 1990. Two-stage decompression in orthopyroxene–sillimanite granulites from Forefinger Point, Enderby Land, Antarctica: implications for the evolution of the Archaean Napier Complex. J. Metamorph. Geol. 8, 591–613.

Hensen, B.J., 1987. P–T grids for silica-undersaturated granulites in the systems MAS (n+4) and FMAS (n+3) — tools for the derivation of P–T paths of metamorphism. J. Metamorph. Geol. 5, 255–271.

Hensen, B.J., Harley, S.L., 1990. Graphical analyses of P–T–X relations in granulite facies metapelites. In: Ashworth, J.R., Brown, M. (Eds.), High Temperature Metamorphism and Crustal Anatexis. Unwin Hyman, pp. 19–56.

Jain, S.C., Yedekar, D.B., Nair, K.K.K., 1991. Central Indian shear zone: a major Pre-Cambrian crustal boundary. J. Geol. Soc. (India) 37, 521–531.

Jain, S.C., Nair, K.K.K., Yedekar, D.B., 1995. Geology of the Son–Narmada–Tapti lineament zone in Central India. Geoscientific studies of the Son–Narmada–Tapti Lineament Zone: Geological Survey of India Special Publication, vol. 10, pp. 1–154.

Kelly, N.M., Harley, S.L., 2004. Orthopyroxene–corundum in Mg–Al-rich granulites from the Oygarden Islands, East Antarctica. J. Petrol. 45, 1481–1512.

Kovach, V.P., Simmat, R., Rickers, K., Berezhnaya, N.G., Salnikova, E.B., Dobmeier, C., Raith, M.M., Yakovleva, S.Z., Kotov, A.B., 2001. The Western Chamockite Zone of the Eastern Ghats Belt, India — an independent crustal province of late Archaean (2.8 Ga) and Palaeoproterozoic (1.7–l.6 Ga) terrains. International Symposium and Field Workshop on the Assembly and Breakup of Rodinia and Gondwana, Osaka, 26–30 October 2001. Gondwana Res. 4, 666–667.

Kretz, R., 1983. Symbols for rock-forming minerals. Am. Mineral. 68, 277–279.

Lindsley, D.H., 1983. Pyroxene thermometry. Am. Mineral. 68, 477–493.

McDade, P., Harley, S.L., 2001. A petrogenetic grid for aluminous granulite facies metapelites in the KFMASH system. J. Metamorph. Geol. 19, 45–59.

Mezger, K., Cosca, M.A., 1999. The thermal history of the Eastern Ghats Belt (India), as revealed by U–Pb and ^{40}Ar–^{39}Ar dating of metamorphic and magmatic minerals: implications for the SWEAT correlation. Precambrian Res. 94, 251–271.

Mishra, D.C., Singh, B., Tiwari, V.M., Gupta, S.B., Rao, M.B.S.V., 2000. Two cases of continental collisions and related tectonics during the Proterozoic period in India — insights from gravity modelling constrained by seismic and magnetotelluric studies. Precambrian Res. 99, 149–169.

Moraes, R., Brown, M., Fuck, R.A., Camargo, M.A., Lima, T.M., 2002. Characterization and P–T evolution of melt-bearing ultrahigh-temperature granulites: an example from the Anápolis-Itauçu Complex of the Brasília Fold Belt, Brazil. J. Petrol. 43, 1673–1705.

Motoyoshi, Y., Hensen, B.J., 1989. Sapphirine–quartz–orthopyroxene symplectites after cordierite in the Archaean Napier Complex, Antarctica: evidence for a counterclockwise P–T path? Eur. J. Mineral. 1, 467–471.

Motoyoshi, Y., Matsueda, H., 1984. Archean granulites from Mt. Riiser-Larsen in Enderby Land, East Antarctica. Memoirs of the National Institute of Polar Research, Special Issue, vol. 33. National Institute of Polar Research, Tokyo, pp. 103–125.

Mouri, H., Guiraud, M., Hensen, B.J., 1996. Petrology of phlogopite–sapphirine-bearing Al–Mg granulites from Ihouhaouene, In Ouzzal, Hoggar, Algeria: an example of phlogopite stability at high temperature. J. Metamorph. Geol. 14, 725–738.

Nair, R., Chacko, T., 2002. Fluid-absent melting of high-grade semipelites: P–T constraints on orthopyroxene formation and implications for granulite gneiss. J. Petrol. 43, 2121–2141.

Naqvi, S.M., Rogers, J.J.W., 1987. Precambrian Geology of India. Oxford University Press, New York. 223 pp.

Ouzegane, K., Bouzame, S., 1996. An example of ultrahigh-temperature metamorphism: orthopyroxene–sillimanite–garnet, sapphirine–quartz and spinel–quartz parageneses in Al–Mg granulites from In Hihaou, In Ouzzal, Hoggar. J. Metamorph. Geol. 14, 693–708.

Ouzegane, K., Guiraud, M., Kienast, J.R., 2003. Prograde and retrograde evolution in high-temperature corundum granulites (FMAS and KFMASH systems) from In Ouzzal terrane (NW Hoggar, Algeria). J. Petrol. 44, 517–545.

Pattison, D.R.M., Harte, B., 1985. A petrogenetic grid for pelites in the Ballachulish and other Scottish thermal aureoles. J. Geol. Soc. (London) 142, 7–28.

Pattison, D.R.M., Harte, B., 1991. Petrography and mineral chemistry of pelites. In: Voll, G., Topel, J., Pattison, D.R.M., Seifert, F. (Eds.), Equilibrium and Kinetics in Contact Metamorphism: The Ballachulish Igneous Complex and its Aureole. Springer Verlag, Heidelberg, pp. 135–180.

Pattison, D.R.M., Chacko, T., Farquhar, J., McFarlane, C.R.M., 2003. Temperatures of granulite facies metamorphism: constraints from experimental phase equilibria and thermobarometry corrected for retrograde exchange. J. Petrol. 44, 867–900.

Raith, M., Karmakar, S., Brown, M., 1997. Ultra-high-temperature metamorphism and multistage decompressional evolution of sapphirine granulites from the Palni Hill ranges, southern India. J. Metamorph. Geol. 15, 379–399.

Sajeev, K., Osanai, Y., 2004. Ultrahigh-temperature metamorphism (1150 °C, 12 kbar) and multistage evolution of Mg-, Al-rich granulites form the central Highland Complex, Sri Lanka. J. Petrol. 45, 1821–1844.

Sajeev, K., Osanai, Y., Santosh, M., 2004. Ultrahigh-temperature metamorphism followed by two-stage decompression of garnet–orthopyroxene–sillimanite granulites from Ganguvarpatti, Madurai block, southern India. Contrib. Mineral. Petrol. 148, 29–46.

Sandiford, M., Powell, R., 1986. Pyroxene exsolution in granulites from Fyfe Hills, Enderby Land, Antarctica: evidence for 1000 °C metamorphic temperatures in Archean continental crust. Am. Mineral. 71, 946–954.

Sandiford, M., Neall, F.B., Powell, R., 1987. Metamorphic evolution of aluminous granulites from Labwor Hills, Uganda. Contrib. Mineral. Petrol. 95, 217–225.

Santosh, M., Yokoyama, K., Acharyya, S.K., 2004. Geochronology and tectonic evolution of Karimnagar and Bhopalpatnam Granulite Belts, Central India. Gondwana Res. 7, 501–518.

Sarkar, S.N., Trivedi, J.R., Gopalan, K., 1981. New data on the geochronology of the Precambrians of Bhandara-Drug, Central India. Ind. J. Earth Sci. 8, 131–151.

Sarkar, G., Ray Barman, T., Corfu, F., 1989. Timing of continental arc magmatism in northwest India: evidence from U–Pb Zircon geochronology. J. Geol. 97, 607–612.

Sengupta, P., Dasgupta, S., Bhattacharya, P.K., Fukuoka, M., Chakraborti, S., Bhowmik, S., 1990. Petrotectonic imprints in the sapphirine granulites from Anantagiri, Eastern Ghats Mobile Belt, India. J. Petrol. 31, 971–996.

Sengupta, P., Sen, J., Dasgupta, S., Raith, M., Bhui, U.K., Ehl, J., 1999. Ultra-high temperature metamorphism of metapelitic granulites from Kondapalle, Eastern Ghats Belt: implications for the Indo-Antarctic correlation. J. Petrol. 40, 1065–1087.

Srogi, L., Wagner, M.E., Lutz, T.M., 1993. Dehydration partial melting and disequilibrium in the granulite-facies Wilmington Complex, Pennsylvania-Delaware Piedmont. Am. J. Sci. 293, 405–462.

Topuz, G., Altherr, R., Kalt, A., Satir, M., Werner, O., Schwarz, W.H., 2004. Aluminous granulites from the Pulur complex, NE Turkey: a case of partial melting, efficient melt extraction and crystallization. Lithos 72, 183–207.

Waters, D.J., 1986. Metamorphic history of sapphirine-bearing and related magnesian gneisses from Namaqualand, South Africa. J. Petrol. 27, 541–565.

Waters, D.J., 1989. Metamorphic evidence for the heating and cooling path of Namaqualand granulites. In: Daly, J.S., Cliff, R.A., Yardley, B.W.D. (Eds.), Evolution of Metamorphic Belts: Geol. Soc. London, Spec. Publ., vol. 43, pp. 357–363.

White, R.W., Powell, R., Halpin, J.A., 2004. Spatially-focussed melt formation in aluminous metapelites from Broken Hill, Australia. J. Metamorph. Geol. 22, 825–845.

Yedekar, D.B., Jain, S.C., Nair, K.K.K., Dutta, K.K., 1990. The Central Indian collision suture. Precambrian of Central India: Geological Survey of India Special Publication, vol. 28, pp. 1–37.